Chapter 4

MODEL DEVELOPMENT I

Regression analyses

The previous chapter describes a series of experimental programs, each providing some data and relationships which should be useful in modelling the forces involved in penetrating a ridge keel. In this chapter results from the experiments in Chapter 3 have been combined with data from the literature for regression analyses. The grouped data sets include those for ridge keel shape, ice rubble shear strength and structure interaction forces. Any individual test program tends to involve a choice of a limited set of parameters which are varied, and often a limited range over which variation occurs. When diverse programs are studied collectively, general results are obtained, removing or reducing biases which result from the limitations of any one test procedure. While collective studies run the risk of oversimplifying some issues they can broaden the applicability of results and, as the following shows, can be a better guide for future work.

4.1 First-year ridge keel shape

Though there have not been any new field data presented in this thesis, this section describes the results of a new regression study of ridge keel shape. The data used are described in the thesis background as reported in Burden and Timco (1995). Burden and Timco (1995) catalogued the dimensions of over 112 first-year and 64 multi-year ridges. The first-year ridges were divided into two groups: those associated with temperate

climates and those from the arctic. The keel data for temperate first-year ridges were considered in this study.

Detailed surveys of ridge cross-sections have shown that keel shapes have varying slopes with both convex and concave curvature. The keel bottom may be pointed and off-centre, rounded or flat. Naturally, there are no simple geometric forms that perfectly define all ridges. For analytical modelling, ridges are typically categorized as triangular or trapezoidal in cross-section because those shapes are easily defined by measured field data; usually width, depth and sometimes slope angle. Though commonly applied, these shapes present some analytical difficulties since they possess slope discontinuities. Discontinuities preclude one from defining the whole keel with a simple, single algebraic formula, a convenience for computing depth across the entire ridge. For this study the replacement of the facetted geometric approximations with that of a half-cycle "sine wave" form has been considered (Figure 4.1). To investigate the quality-of-fit of the "sine" approximation the data sets presented by Burden and Timco have been reanalysed.

Keel width to depth ratio

A total of 44 ridges had both keel width and depth measurements studied. A regression analysis was performed to determine the best linear and non-linear relationship between these measured parameters. The resulting formulas are

$$W = 2.5H + 9.4 \quad \textit{and} \quad W = 9.2H^{0.525} \qquad (1)$$

where W and H are the keel width and depth in meters. For the linear relation the r^2 value, adjusted for degrees of freedom, was 44.8% and the standard deviation of the somewhat normally distributed residuals was 8.2 m. The power-law fit established through a natural log transform had a standard deviation of the normally distributed log residuals of 0.3471 with an adjusted r^2 value of 38.7%. A linear relationship between the width and depth, fitted with a zero intercept as in Burden and Timco (1995), resulted in the relation, $W = 3.99H$ with an r^2 of 24%. Figure 4.2 is a scatter plot of the ridge data with both fitted linear relations and the power law fit.

Keel angle

Both fore and aft keel angles are listed in Burden and Timco (1995). These terms are understood to be used arbitrarily assigned to differentiate between the two slopes of a given ridge and are in no way a convention for classifying any particular ridge orientation. The method of measurement is not recorded. For 16 first-year temperate region ridges the averages of the angles which were measured are 28.8° and 26.3° respectively, resulting in an overall average of 27.5°. Of the 16, only 8 ridges had width and depth stated. If these 8 ridges were assumed to be either triangular or "sine" shaped, the average slope angle for both is found to be 23.5°, a slight underestimate of the measured average (the average angle for both shapes is computed from the arctan of ridge depth over half the ridge width). The relation between measured and computed slope is investigated further in Figure 4.3. Although both shapes have the same average slope over a half length, the slope of the "sine" shape varied between 0.0 and 33.5° from tip to toe. This range encompasses the measured values above.

Keel area

Through digitization, Burden and Timco determined the cross-sectional area of 18 temperate first-year ridges. Only six of these corresponded to ridges for which both width and depth data were also provided. Width and depth dimensions were estimated from digitized plots so that another 11 of the 18 ridges could be considered in this study. The area under a "sine" shaped approximation ($2HW/\pi$) over-estimates the measured areas by 12%. The area under an isosceles triangle of equal proportions underestimates areas by the same margin (Figure 4.4). When only the six fully-defined ridges are used, the error for the "sine" approximation diminishes to 7% and that for triangular keels increases to 14%.

The "sine" keel shape is a more accurate keel cross-sectional area shape approximation than the isosceles triangle one. When one considers that overstating size results in overestimated loads, which is safer than underestimating, the new "sine" shape may be a better choice for design regardless of the improvement. Further, the continuous and simple form of the "sine" curve may indeed provide easier load modelling by eliminating slope discontinuities[1].

[1] Brown and Bruce (1995) conducted a finite element investigation of the stress distribution within a ridge keel during indentation. In that study the stress patterns/contours below the surface of a triangular keel were shown to be parabolic or *sine*-like in shape. This indicated that discontinuities in surface form did not translate to internal stress discontinuities.

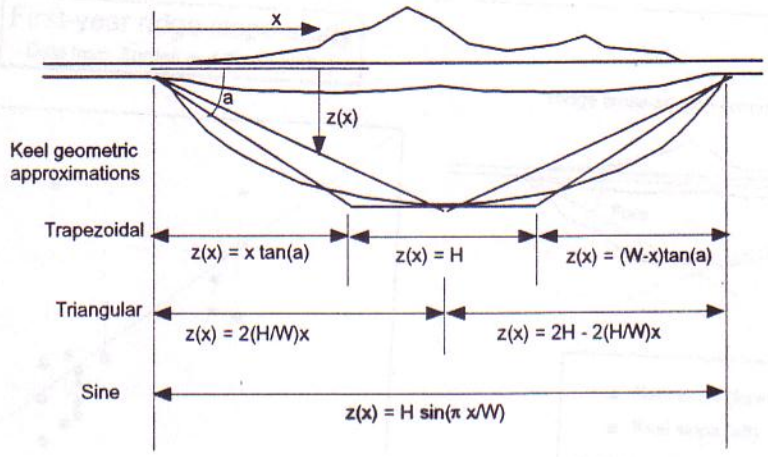

Figure 4.1 Keel geometry approximations.

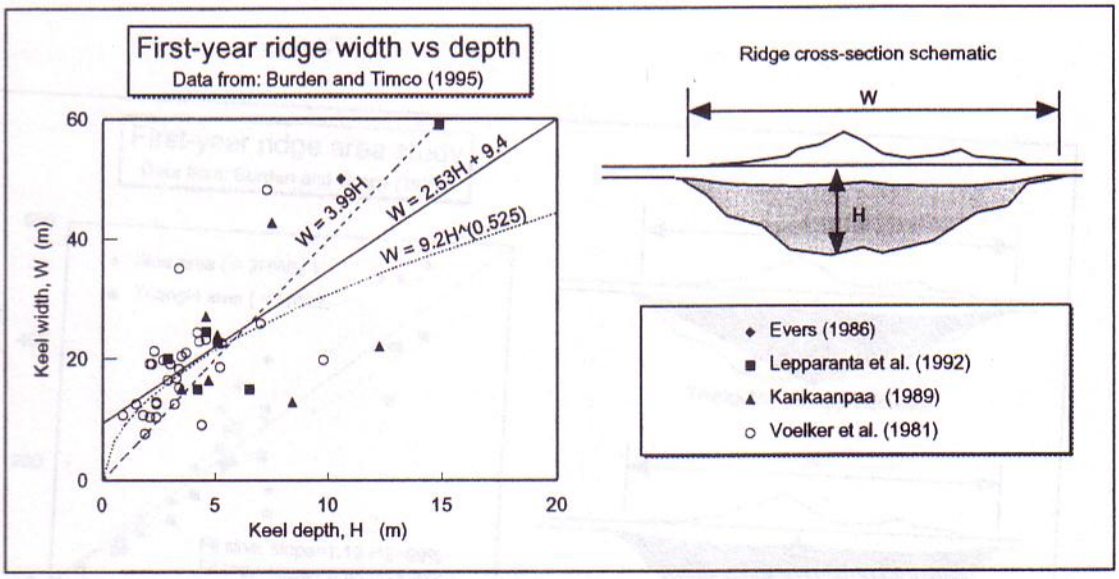

Figure 4.2 Keel width vs depth study.

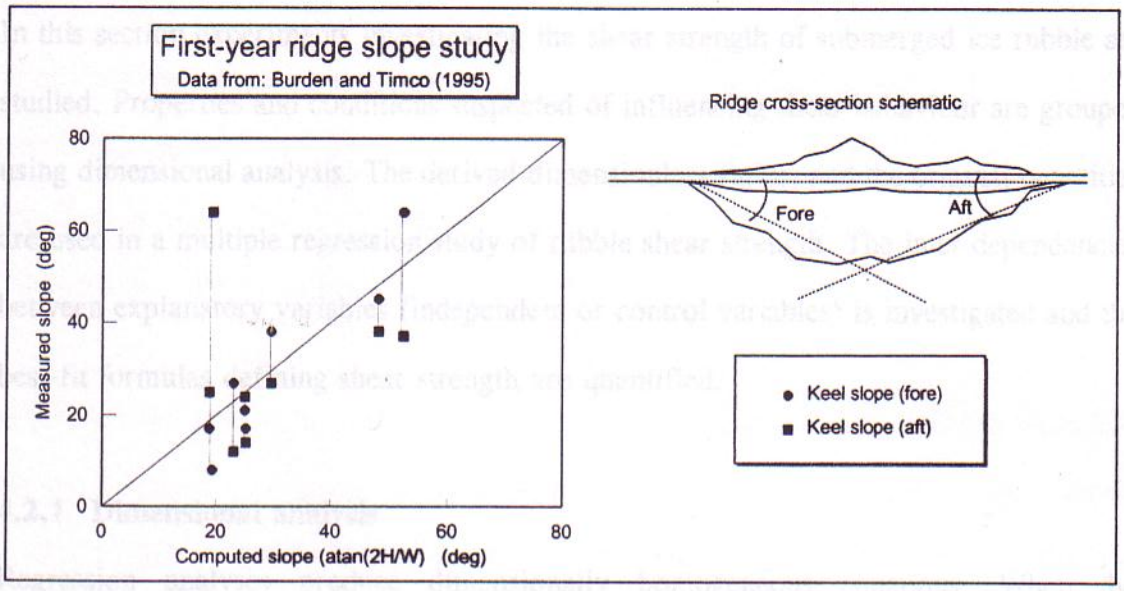

Figure 4.3 Keel slope study.

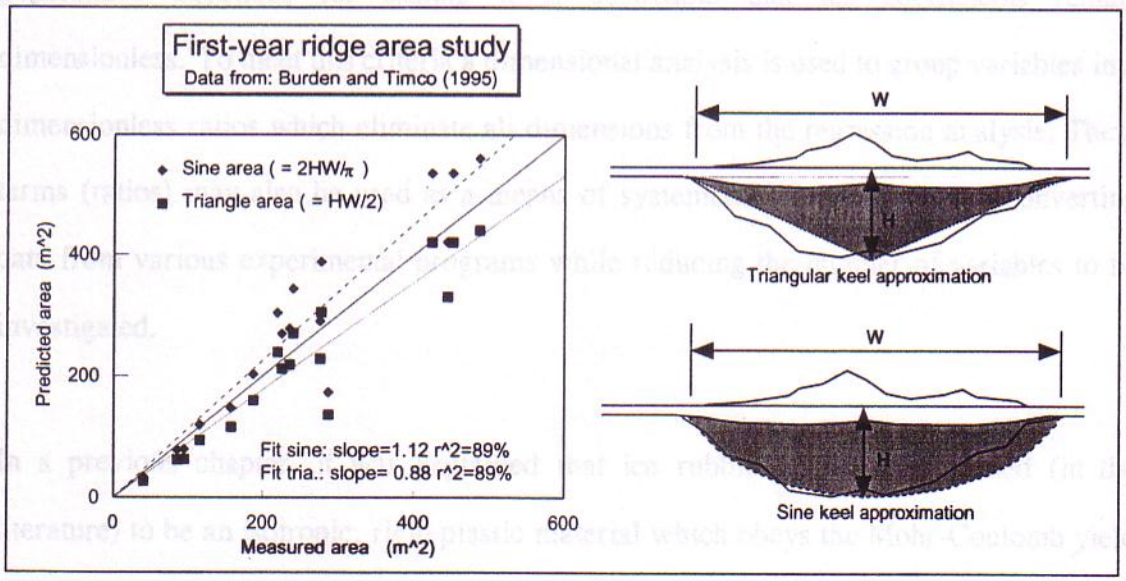

Figure 4.4 Keel cross-sectional area study.

4.2 Ice rubble shear strength

In this section experiments investigating the shear strength of submerged ice rubble are studied. Properties and conditions suspected of influencing shear behaviour are grouped using dimensional analysis. The derived dimensionless ratios, and the original quantities are used in a multiple regression study of rubble shear strength. The inter-dependencies between explanatory variables (independent or control variables) is investigated and the best-fit formulas defining shear strength are quantified.

4.2.1 Dimensional analysis

Regression analyses produce dimensionally homogeneous equations. When the dimensions of control variables on both sides of an equation are not similar, the regression coefficients assume a dimensional form. When developing and classifying generalized equations for scaling it is desireable that the coefficients remain dimensionless. To meet this criteria a dimensional analysis is used to group variables into dimensionless ratios which eliminate all dimensions from the regression analysis. These terms (ratios) may also be used as a means of systematically collecting and converting data from various experimental programs while reducing the number of variables to be investigated.

In a previous chapter, it was explained that ice rubble is broadly assumed (in the literature) to be an isotropic, rigid plastic material which obeys the Mohr-Coulomb yield criterion. Consequently, the shear strength is said to arise from independent frictional and cohesive components. Friction in a granular material arises from interlock, block strength

and surface friction. The conditions which influence friction behaviour include packing density, block shape, size, and gradation, surface roughness, the presence of surface water, particle composition and particle strength. Cohesion in a bulk ice rubble sample was shown to be a function of the freeze-bonding propensity of the ice and would, therefore, be dependent upon heat transfer, block scale, contact pressure, ice impurities, shearing rate, interstitial fluid and other factors.

As pointed out in section 3.3 it appears that the fundamental Mohr-Coulomb plasticity assumption stated above oversimplifies the true nature of ice rubble (Ettema and Urroz-Aguirre, 1991). Due to the apparent stress dependency of ϕ and c terms, and for completeness in the dimensional analysis, both are grouped here with all other explanatory variables for the broadest possible analysis.

The hypothesis tested in the dimensional analysis is

$$\phi, c = f(L_x,\ L_i,\ t,\ S,\ e,\ V,\ \gamma,\ \sigma_{fl},\ \sigma_{max}) \qquad (40)$$

with terms defined as follows:

- block size, median of maximum dimension L_x, and minimum dimension L_i,
- duration, t, of contact between blocks within the bulk sample,
- interstitial water impurity content (salinity mostly), S,
- porosity of bulk sample, e,
- shear speed, V,
- rubble buoyant weight, γ,
- ice block flexural strength, σ_{fl},
- and maximum confinement stress, σ_{max}.

The preceding list was developed after consideration of the various reporting methods and experimental procedures in the literature. Not all of the factors expected to assert some influence can be included in this listing. For instance, temperature and particle grading are omitted due to the absence of reported information. However, while contact duration, t, was poorly reported it does appear in the analysis to ensure that one other significant variable, in addition to velocity, which involves time is included. Its value is set to unity for all data sets as a default value.

Flexural strength was selected (instead of another ice strength index) primarily because it was the most commonly reported ice strength parameter in the literature for rubble shear strength. It may be argued that for *platy* blocks, failure in flexure will occur at lower stresses than pure crushing or tension in an interlocked matrix of blocks being sheared. Under these circumstances flexural strength may be the better choice since it would be closely tied to any threshold for non-linear shear behaviour. Regardless, flexural strength would be significantly related to the other strength indices - thus a regression equation with either strength index would probably have the same parametric significance(s) but possess different coefficients of proportionality.

Figure 4.5 shows the workings of the *matrix technique* for dimensional analysis. This technique (described in Sharp *et al.*, 1992) enables the systematic evaluation of many Π parameters objectively and completely even when large numbers of variables are involved. The dimensionless groups ultimately chosen using this process are as follows:

$$\phi, \frac{c}{\sigma_{fl}} = f\left[\frac{\gamma L_x}{\sigma_{fl}}, \frac{Vt}{L_x}, S, e, \frac{L_x}{L_i}, \frac{\sigma_{max}}{\sigma_{fl}}\right] \qquad (41)$$

These are selected because of their physical significance and prior use in the literature. Sensitivity runs confirm the validity of this selection, in particular, the use of flexural strength as a repeating variable for normalization. Both σ_{max} and γL_x were substituted for flexural strength resulting in dimensionless parameters which ultimately yielded poorer correlations than those listed above.

4.2.2 Analysis data set

The values of explanatory variables from all the sources used in the study are listed in Table 4.1. Friction angle and cohesion are usually stated in each literature reference, only a few values are computed here from plotted data. Ordinarily, block size is given, though dimensions are often approximate. The "maximum" block size described by most researchers is typically the average or median of the longest dimension of blocks and not the largest block in the bulk sample. Block thickness (median of minimum block dimension, L_i) and median of the maximum block dimension, L_x, are used independently in this study since it is uncertain which is more important, and the ratio of the two gives an indication of particle shape. The rate of shearing is reported quantitatively in all but one reference. Keinonen and Nyman (1978) use the relative term, "slowly by hand" which is estimated here to be around 25 mm/sec. Some references do not cite a flexural strength for the ice used in tests. Where this is the case values are estimated based on the description of the ice. For instance, freshwater ice near 0° C is assigned a flexural strength of 1 MPa after work by Gow (1977).

The salinity of the fluid in which the rubble is immersed is known to significantly affect ice rubble freeze-bonding (Schaefer and Ettema, 1986). Outside of a laboratory one would expect salinity and flexural strength to be too closely correlated to be considered

independent for multiple regression purposes. However, in the lab flexural strength is controlled to a large extent by the air content of the ice. Bubble layering and spraying are two techniques used to enhance the void ratio of ice allowing flexural strength scaling. Some laboratories use chemical dopants such as urea and EG/AD/S as a substitute for salts. A control experiment has not been done to investigate the effects of these dopants on the freeze-bonding of ice blocks. It is assumed here that the influences of all dopants (salts included) is proportional to the percent weight of the impurity in the water. Experiments in freshwater are assigned an arbitrary impurity of 0.001% since a value of zero prohibits some transformations of variables (logs, square roots, inverses etc.) and is unlikely in any event.

All but two researchers report values of bulk sample porosity. Since porosity is difficult to measure, especially when ice blocks have a lower density out of water when pores drain, the quoted values are usually approximate. Neither Hellmann (1984) or Case (1991) give estimates of bulk porosity so bulk porosity values for those references have been estimated. Since there does not appear to be an obvious relation between porosity and block size, Hellmann's rubble samples are considered here to possess average porosity (35%) as no unusual packing procedures are mentioned. Case (1991) used ice rubble similar to that reported in Section 3.5 (from Bruneau *et al.*, 1996) and so the same value is adopted (30%). The buoyant weight of the rubble sample is computed from bulk porosity, and, ice and water density. Though seemingly correlated, porosity and weight parameters are carried through the dimensional analysis separately and into the regression study, where spurious correlations can be dealt with systematically.

Most rubble shear experiments in the lab involve direct shear devices which produce a

horizontal or vertical failure surface in an ice rubble sample. Where external forces are applied to provide a variation in the normal pressure, stresses from rubble weight or buoyancy are relatively small. Ettema and Urroz-Aquirre (1991) argue that some researchers with vertical direct shear apparati have neglected this buoyant stress which gives rise to a cohesive intercept that should not be there. They suggest that the horizontal confining pressure on a vertical shear plane is

$$\sigma_h < K_p \, \sigma_v \tag{42}$$

where the σ_v is the rubble (buoyant) hydrostatic pressure, σ_h is the horizontal component of this pressure during shearing and K_p is the Rankine passive pressure coefficient. This assertion implies that during shearing the vertical pressure increases by a factor of K_p. In direct shear tests with soil the vertical pressure is not considered to do this as K_p and K_a are not coefficients for pressures on failure planes. For the experiments by Prodanovic (1979), Weiss *et al.* (1981), and Hellmann (1984) as cited in Ettema and Urroz (1989) the normal stress was either regulated at a constant value or measured throughout so as to provide instantaneous coincident shear and normal stress values. Other than the platen used to apply the normal stress only friction on the walls of the shear boxes can provide reaction forces adding to normal stresses on the failure plane. Based on shear box dimensions and construction it is unlikely that any significant stress on the failure plane was not measured as a normal stress. Both Prodanovic and Weiss *et al.* report shear experiments at a confining stress of zero. This is also unlikely, suggesting that either the original static pressure may have been zeroed out of the readings or confinement may have been very low so that it was rounded off to zero. Potentially, the ice rubble may have become self-supporting due to freeze-bonding (cohesion) after being placed in the

shear box so that any relief in the box would relieve measured confinement pressure. For those shear box tests where the failure planes are vertical the reported normal stresses are used here for all but the zero stress data points. A normal stress value equivalent to one-half the average vertical (0.5 σ_v) is used since the rubble would have to have been confined at least that much in the placement process. Where failure planes are horizontal, normal stress values are elevated here by an amount equivalent to the hydrostatic pressure if it does not appear to have been included. The σ_{max} values in Table 4.1 represent the highest normal stress used in each reference in which ϕ and c are computed.

4.2.3 Regression analysis

Multiple regression techniques have been used to synthesize formulas representing the relationship between ϕ, c and the other explanatory variables listed in Table 4.1. Details of the techniques used are described in Lye (1995). The quality of the fitted formulae was determined by analyzing the residuals for patterns and outliers. Variables were transformed when residual plots appeared skewed - indicating that not all data trends have been identified. Most often the natural logarithms of data were used when residuals were heteroscedastic (the spead of residuals increases with the independent variable). Few trends other than convergence and divergence of residuals were encountered. The most pervasive problem with all data sets was multicollinearity or the undesirable condition where at least one explanatory variable is closely related to one or more other explanatory variables. When explanatory variables are significantly correlated, parameter importance and regression formulas are usually distorted and erroneous.

The Minitab software employed in this regression study is capable of flagging highly correlated explanatory variables so some multicollinearity problems were avoided this way. Variable inflation factors which indicate the multi-variable correlation of each explanatory variable against all others were computed also. Threshold acceptability values (from Lye, 1995) were used to accept or reject some variables for various tests. Matrix plots of scatter diagrams and tables of simple regression results were also employed to screen explanatory variable correlations. Also, "forwards" and "backwards" *stepwise regression* techniques which indicate a type of "regression repeatability" were employed to guard against multicollinearity and to register the best $\mathbf{r}^2$ value, adjusted for the number of explanatory variables (degrees of freedom) in use.

The adjusted $\mathbf{r}^2$ value indicates the percentage of the variation in the dependent variable described by the given formula. The partial **F** test, or **t** test, was used to determine the benefit of any one variable to the overall equation. Registering $|\mathbf{t}| > 2.0$ (or $\mathbf{p} < 0.05$) indicates a significantly non-zero influence at the 95% confidence level, (**p** representing the actual probability of not meeting this criterion). Thus $|\mathbf{t}| = 2$ was the threshold for accepting or rejecting a given variable. Since **t** values are often highly sensitive to the subtraction or addition of any variable, many combinations of variables were tested to determine those which avoided multi-collinearity and were significant.

General relationships

The linear correlation coefficients for all pairs of variables are listed in Table 4.2 for dimensional and Table 4.3 for non-dimensional terms. At a glance one can see that significant correlations of variables exist (shaded regions) for the data set in general. Even speed, a seemingly independent parameter, is correlated to other control parameters

in the laboratory. Many correlations can be explained by the habits of experimentalists. For instance, larger labs produce larger ridges with larger blocks at higher confinement. There may or may not be similar trends in the field. This type of correlation should be avoided in the laboratory and must be avoided in multiple regression analysis. Correlations between non-dimensional terms in Table 4.3 are even more difficult to understand and so are best avoided completely.

Cohesion

The relation between apparent cohesion and several explanatory variables was investigated. Both dimensional and non-dimensional forms of cohesion were studied. The analysis was carried out with, and without, ϕ in the list of explanatory variables. All formulas yielding a spreading trend in the residuals were transformed using natural logs and a variety of exponents, where applicable.

The formulas yielding the best-fit, with normalized residuals and with the lowest likelihood of multicollinearity (or correlation error) are listed in Table 4.4. Many other combinations of variables were explored, frequently yielding $\mathbf{r^2}$ values much higher than those listed. However, where explanatory variables are strongly related to each other (as the shaded areas of Table 4.2 and Table 4.3 indicate), only one may be considered.

Figure 4.6 is a plot of the best-fit formulation for the relationship between cohesion and maximum normal stress, both normalized by flexural strength. With an $\mathbf{r^2}$ value of 78.3% this dimensionless equation may be suitable for scaling. Cohesion is strongly correlated to block size in this study. Figure 4.7 indicates the best single variable relationship for cohesion (in Pascals) as

$$c = 16240L_i - 7 \quad (43)$$

where L_i is block thickness (in meters). Apparently, block size is also significantly proportional to the maximum normal stress (see Table 4.2). Thus the relation between block size and cohesion may be influenced by the dependency of cohesion on normal stress or *vice versa*. Table 4.4 identifies the linear and non-linear relationships between cohesion and maximum stress - both yielding $\mathbf{r}^2$ values around 60%.

The regression analysis procedure was repeated with the data sets from Urroz and Ettema (1987), Bruneau (1994a) and McKenna *et al.* (1996) removed. There was no attempt to *improve* results by doing so. These were selected since apparatus and test procedures differed from the rectangular, direct shear devices of the others. Comparing these sensitivity results to the earlier results (both in Table 4.4) shows that moderate increases in $\mathbf{r}^2$ were identified for cohesion, which in the sensitivity study is surprisingly well-defined by block thickness and shear speed (Figure 4.8). The inverse relationship between cohesion and speed may be evidence that cohesive bonds may form relatively fast and that bond strength may be strain-rate dependent.

Internal friction angle

Regression equations resulting from the study of ϕ vs dimensional and non-dimensional parameters are also listed in Table 4.4. Transformation of variables was not required in this case as residuals were normally distributed with linear regression. As Table 4.4 shows the angle of internal friction is influenced by variations in porosity and block size. Figure 4.9 is a scatter plot of the individual relationships and Figure 4.10 is a quality-of-fit diagram for the relation:

$$\phi = (1.22 - 168L_i + 1.37e) \geq 0 \qquad (44)$$

where ϕ is the internal friction angle in degrees, L_i is the block thickness in meters and e is bulk porosity in percent. Both Figures 4.10 and 4.11 demonstrate the apparent weakness of the correlation. The multi-collinearity of maximum normal stress, block size, weight etc. as highlighted in Table 4.2 limited the combinations of parameters possible in the study. Typically around 50% of the variation of ϕ can be explained by one or two explanatory variables. The percentage is higher in the sensitivity run where the elimination of some data sets yields an r^2 of 67.2% for the relation involving cohesion and porosity.

Comments

Apparently, cohesion scales linearly with block thickness, the robust relationship established accounts for around 70% of the variation in c. Taking into account the sensitivity runs, cohesion can be roughly approximated in kPa by $17L_i$, where L_i is the block thickness in meters. The dimensionless ratio c/σ_{fl} is highly correlated to σ_{max}/σ_{fl} (r^2 of 78%) and may be a good choice for scaling cohesion estimates.

Approximately 40% of the scatter in ϕ cannot be accounted for through regression analysis, though porosity appears to be a predominantly significant explanatory variable. Evidently an inverse relation exists between ϕ and c (Table 4.4). This is an indication of a flattening of the Mohr-Coulomb failure envelope at higher mean pressures possibly resulting from particle degradation and the loss of granular shear behaviour.

4.2.4 Shear vs normal stress

The data points from which the ϕ and c terms in Table 4.1 were derived have been collected so that an evaluation of instantaneous shear and normal stress could be made independent of the reported Mohr-Coulomb failure criteria. This study was prompted by the apparent dependency of cohesion and friction angle on normal stress demonstrated in Table 4.2 and Table 4.4.

Figure 4.11 is a plot of shear stress vs normal stress including all data sets used in the previous study. Several other ice rubble shear tests which have been reported in the literature have not been included in the figure. The tests by Wong *et al.* (1987), Sayed (1987), Eranti *et al.* (1992), Cornett and Timco (1996) and others either saw a monotonic increase in shear stress with no specific failure point, involved experiments with dry ice rubble, or were not fully reported. In Figure 4.12 data from Lehmus and Karna (1995) and Cheng and Tatinclaux (1977) have been added to the data from Figure 4.11. From both Figures 4.11 and 4.12 it appears that a lower boundary shear strength exists that it is slightly concave/parabolic. The upper boundary of data appears to be defined by some radical outliers from the data sets of Lehmus and Karna (1995) and also Bruneau (1994a) who were studying consolidation effects, as well as Cheng and Tatinclaux (1977) where there was no attempt to control or measure normal stress (estimated here from rubble depth), and by Weiss *et al.* (1981) who used the largest apparatus and ice blocks. From Figure 4.13 where data is grouped according to ice temperature, speed and contact period it appears that the upper bound may be a feature of cold ice or extended contact.

Since many properties of ice, including strength, vary according to the salinity of the solution in which it is formed it was of interest to discriminate between tests using either

saline, fresh or doped ice. Figure 4.14 provides no particular insights, however, as data for all three types of ice are scattered somewhat evenly.

A dimensional analysis was performed in which the terms for shear and normal stresses, τ and σ_n, were substituted for ϕ, c and σ_{max}. Figure 4.15 indicates the matrix methodology used to formulate dimensionless ratios. Normal stress was selected as a repeating variable instead of flexural strength allowing the dimensionless ratio between shear and normal stress to arise. The derived expression is:

$$\frac{\tau}{\sigma_n} = f\left[\frac{\gamma L_x}{\sigma_{fl}}, \frac{\sigma_{fl}}{\sigma_n}, \frac{Vt}{L_x}, S, e, \frac{L_x}{L_i}\right] \qquad (45)$$

Again, multiple regression techniques have been used to synthesize formulas representing the relationship between τ and those explanatory variables as they appear in dimensionless groups above. The base data set used in this study is limited to those for which values of ϕ and c were known in Table 4.1. This means that Lehmus and Karna (1995), and, Cheng and Tatinclaux (1977) were not included. A sensitivity study was carried out later in which these tests were included. The table listing all data point values appears in Appendix A.

Linear regression results for dimensional and non-dimensional terms are tabulated in Table 4.5 and Table 4.6 respectively. For very large data sets the **t** test of significance is not meaningful so only $\mathbf{r}^2$ (adjusted) has been used as a guide for simple correlation and variance inflation factors were once again used to avoid multi-collinearity.

Table 4.7 lists the multiple regression results. Linear and non-linear relations between

τ and σ_n were determined. The distributions of residuals were typically log-normal indicating that a power-law relation for the combined data set was more appropriate than a linear fit. The best power-law fit relationship for shear stress was determined as:

$$\tau = \frac{(\sigma_n)^{0.878}\ (e)^{0.55}}{(\sigma_{fl})^{0.0851}} \qquad (46)$$

with an r^2 of 80% where all stresses are in Pascals and porosity, e, is in percent. Including Lehmus and Karna (1995), and, Cheng and Tatinclaux (1977) considerably worsened the correlation. Eliminating the "non-standard" direct shear data sets (Urroz and Ettema, 1987, Bruneau, 1994a, and McKenna *et al.*, 1996) did not improve the relation either. Figure 4.16 is a plot of the base data set with the best linear and non-linear single variable correlations shown. The approximate strength of solid ice and loose sand are also plotted as a reference for relative strength. The range of maximum normal stress typical for ridges between 5 and 20 m deep is also plotted so that one may quickly recognise the region of the graph which is of the greatest practical importance for keel modelling.

The best linear fit for ice rubble shear strength yields a friction angle of 31° which is approximately equivalent to that of loose sand. It is conceivable that, in a virtually cohesionless state and with favourable grading and particle size, ice rubble behaves as any other blocky granular material. Invariably though, bonding takes place, the degree to which depends on a great many factors. The average appears to be around 590 Pa (from the linear fit on Table 4.7), however, in the figure one can see cohesion up to 5 kPa was observed in the laboratory and may conceivably reach many times higher according to the degree of consolidation (potentially approaching that of solid ice). The

degree of variation is somewhat masked by the logarithmic representation. A band which covers the main swath of the data points is approximately half an order of magnitude in thickness. Overall, the plot of shear vs normal stress in Figure 4.16 illustrates that ice rubble shear strength is strongly related to normal stress but, is also highly variable.

The significant portion of scatter left unexplained by the preceding analysis underscores the sensitivity of ice rubble shear strength to parameters not reported, differing experimental techniques and natural variability. Measurement error is probably responsible for as much as 10 to 20% of the scatter. As described earlier some of the data used in the analysis was inferred or estimated. This may also have contributed to scatter.

4.2.5 Sensitivity study and comparison to full-scale

The empirical formulas for c, ϕ and τ (Equations 43, 44 and 46) described earlier in this section have been evaluated in a sensitivity study shown in Figure 4.17. Two approaches to calculating rubble shear strength are considered. The "phi-c" approach refers to the use of Mohr-Coulomb criteria (ϕ and c from equations 44 and 43), and the "tau" approach which refers to the fundamental shear (τ) vs normal stress relationship (equation 46). The values of explanatory variables selected in the table accompanying the figure are representative of those of a design ridge in temperate climatic zones. The sensitivity study focusses on the relative effect of porosity, block thickness and keel depth as well as comparing the computed shear strength from both approaches. The average shear strength is assumed here to be that at $2H/3$ from the keel bottom, according to a linear hydrostatic approximation. The horizontal bar graph shows that the "tau" model generally produces higher shear strength estimates than the "phi-c" approach. It is also more

sensitive to keel depth, less sensitive to porosity and does not vary with block thickness. For the "phi-c" approach the extrapolation of laboratory results to the field has apparently resulted in remarkably low estimates of friction angle.

A comparison of computed and measured full-scale rubble shear strengths is reviewed in Figure 4.18. Computed values are compared here with those of Lepparanta and Hakala (1992). In that study the investigators performed a detailed study of ridge keel geometry and composition. Five ridge keels were "punch-sheared" vertically with a 2 m square loading platform to obtain shear resistance. Loads were applied using pumped water, concrete block placement and a hydraulic ram. The first technique failed due to the cumbersome handling of the volume of water required. The second was found to be effective for small and medium ridge keels but again became too difficult to handle for larger ridges. The last technique showed the most promise for larger keels though limited stroke and hydraulic pressure prevented complete ridge keel failure.

In the successful punch tests failure planes were vertical and shear resistance measured from 1.7 to 4+ kPa for keels ranging in depth from 2.3 to 11.7 m. Loading period averaged about 2 hours and displaced the keels less than 0.1 m on average which translates to less than 1 mm per minute. This very slow rate is not representative of the conditions under which the highest failure loads are expected to occur. None-the-less, Lepparanta and Hakala claim that the field results have been backed by both shear box and square punch tests performed in the laboratory. The shear strength in the laboratory was said to vary from 0.9 to 2.6 kPa with a mean friction angle of 8.4 degrees. These results are somewhat puzzling since a calculation based upon information given shows that normal stress varied by as much as 0.34 to 1.5 kPa and shear stress varied from 0.9

to 2.6 kPa. This would suggest a friction angle much higher than that stated.

Figure 4.17 indicates that the "phi-c" computed shear strength provides a closer estimate of the full-scale data than the alternate "tau" appraoch. The average errors of the estimates were 17% and 33% respectively. The near match for experiment No. 6 is problematic for the "phi-c" approach, however, since the ultimate shear strength of the ridge was not achieved and may not have been approached in that test. In this case the estimate based on the empirical τ formula may be better.

Lavender (1973) also proposed a full-scale cohesion for ice rubble from river ice jams. The technique used for his estimate of 0 to 3800 Pa is not published and conditions are not known. Regardless, the upper bound is certainly of the same order as that in Figures 4.17 and 4.18.

Hudson (1983) describes full-scale observations of extruded first-year ice ridges in the arctic. Ridge extrusion is described as a phenomenon which occurs when there is a high speed collision between flows or ridges and stationary structures. The formation which develops resembles a deflected ocean wave "frozen" in time. The impression of intense pressures and considerable shearing within the rubble body is given. The extruded crests are somewhat circular in shape implying a "virtually cohesionless" material, according to Hudson.

Hudson points out that a 2 m thick ice sheet produces the same size ice rubble as a 5 m thick sheet which suggests that first-year ridge cohesion may reach some asymptotic limit that could be in the range of 25 to 35 kPa for severe arctic first-year ridges. These

estimates are highly consistent with the block size relation for cohesion here.

At present, the limited data from the field appear to support the prediction of ice rubble shear strength using Mohr-Coulomb failure criteria obtained in the laboratory. Considerable caution should be exercised in doing so, however. As was mentioned in Chapter 2, first-year ridge keel rubble, over long contact periods, may undergo many changes via erosion, freezing, creep, brine transport, melting etc. These processes have not been, and cannot be, adequately modelled in the laboratory so that the range of reported shear strengths may not be fully representative of field conditions. To provide reliable parametric input for ridge keel models it is imperative that efforts be placed in field studies, through methods such as the *in situ* direct shear technique suggested in Section 3.5.

Table 4.1 Laboratory ice rubble shear data for regression analysis.

Reference	Friction angle ϕ deg	Cohesion c Pa	Block thickness Li m	Block length Lx m	Shear Speed V m/s	Block Flexural strength σ_{fl} Pa	Pore fluid salinity S % wt	Bulk porosity e %	Buoyant weight γ N/m^3	Maximum Normal stress σ_{max} Pa
Keinonan and Nyman (1978)	47	11.3	0.02	0.064	0.025	15000	0.6	35	669	1470
Prodanovic (1979)	47	250	0.019	0.152	0.000106	19500	5.5	37.5	735	2710
	53	560	0.038	0.294	0.001185	17500	5.5	37.5	735	2710
Weiss et al. (1981)	34	4100	0.2	0.6	0.005	83000	5.5	45	647	29000
	24	3400	0.2	0.6	0.025	83000	5.5	45	647	21000
	26	2300	0.15	0.45	0.003	55000	5.5	31	812	25000
	25	1400	0.15	0.45	0.024	55000	5.5	31	812	21000
	13	1700	0.08	0.24	0.004	45000	5.5	27.5	853	31000
	11	1200	0.08	0.24	0.025	45000	5.5	27.5	853	8000
Hellmann (1984)	54	580	0.01	0.025	0.0109	1000000	0.001	35	542	3200
	61	420	0.01	0.025	0.0016	1000000	0.001	35	542	3250
	44	280	0.025	0.055	0.0107	1000000	0.001	35	542	4220
	64	1	0.005	0.015	0.0107	50000	0.5	35	574	1800
Fransson&Sandkvist (1985)	34	550	0.039	0.18	0.01	1000000	0.001	20	667	1600
	14	450	0.046	0.15	0.01	780000	0.001	20	667	3000
	13	240	0.008	0.07	0.01	37000	0.6	20	706	850
Urroz and Ettema (1987)	34	1	0.038	0.095	0.002	1000000	0.001	36	533	260
	51	1	0.016	0.038	0.002	1000000	0.001	39	508	480
	38	1	0.018	0.018	0.002	1000000	0.001	23	642	380
	27	1	0.038	0.095	0.002	1000000	0.001	41	492	170
	55	1	0.038	0.038	0.002	1000000	0.001	40	500	290
	33	1	0.018	0.018	0.002	1000000	0.001	31	575	410
	49	1	0.016	0.038	0.002	1000000	0.001	40	500	290
	39	1	0.018	0.018	0.002	1000000	0.001	36	533	310
Case (1991)	48.9	523	0.03	0.096	0.001	34400	0.5	30	446	1780
	37.6	597	0.03	0.096	0.001	27500	0.5	30	446	1630
	34.8	674	0.03	0.096	0.001	19750	0.5	30	446	2400
	27.2	824	0.03	0.096	0.001	15800	0.5	30	446	1500
Bruneau (1994a)	54	2460	0.018	0.035	0.001	2000000	0.001	40	588.6	1250
	59	720	0.018	0.035	0.001	1000000	0.001	40	588.6	1250
McKenna et al. (1996)	36	438	0.05	0.153	0.07	25000	0.5	26	784	625
Bruneau et al. (1996)	41	873	0.04	0.123	0.021	30000	0.5	30	687	2050

Table 4.2 Explanatory variable correlation analysis for ϕ and c terms.

Friction angle ϕ	Cohesion c	Block thickness Li	Block length Lx	Shear Speed V	Flexural strength σ_{fl}	Pore fluid salinity S	Bulk porosity e	Buoyant weight γ	Maximum normal stress σ_{max}
4.8 -1.63 0.112									
18.1 -2.88 0.007	70.1 8.58 0								
17 -2.78 0.009	65.3 7.94 0	92.7 20.43 0							
0 -0.88 0.388	0 0.37 0.716	2.2 1.32 0.198	1.8 1.26 0.216						
6.5 1.82 0.078	1.4 -1.21 0.236	11.2 -2.27 0.03	19.6 -3.01 0.005	10.3 -2.19 0.036					
12.2 -2.36 0.024	37.4 4.55 0	53.8 6.27 0	68.3 8.49 0	0 0.5 0.621	26.4 -3.58 0.001				
17.3 2.82 0.008	6.4 1.81 0.08	1.8 1.27 0.214	0 1.01 0.322	9.4 -2.1 0.044	3 1.42 0.165	0 0.99 0.33			
15.7 -2.67 0.012	8 1.97 0.058	16.7 2.76 0.01	24.4 3.41 0.002	22.2 3.27 0.003	13.9 -2.51 0.017	43.1 5.1 0	9.3 -2.09 0.044		
17.4 -2.82 0.008	61.2 7.28 0	73.6 9.64 0	68.7 8.57 0	0 0.3 0.764	10.5 -2.21 0.034	60.8 7.22 0	0 0.85 0.4	24.7 3.44 0.002	

Key

r^2 adj
t-ratio
p

r^2 adjusted for the number of explanatory variables
|t| > 2 = significant
p < 0.05 means significant within 95% confidence limits
Shading represents significant correlation

Table 4.3 Dimensionless explanatory variable correlation analysis for ϕ and c terms.

ϕ	c/σ_{fl}	$\gamma Lx/\sigma_{fl}$	(V*t)/Lx	σ_{max}/σ_{fl}	S	e	Lx/Li
13.2 -2.45 0.02							
1.7 -1.26 0.219	47.2 5.52 0						
7.6 1.93 0.063	8 -1.97 0.058	2 -1.3 0.204					
0 0.44 0.662	24.5 -3.43 0.002	19.8 -3.02 0.005	1.1 -1.16 0.253				
12.2 -2.36 0.024	42.2 5.01 0	71.9 9.24 0	4.3 -1.58 0.124	13.4 -2.47 0.019			
17.3 2.82 0.008	0 0.25 0.807	0 0.45 0.654	0 -0.93 0.357	7.6 1.93 0.063	0 0.99 0.33		
0 -0.92 0.363	1.7 1.25 0.219	27 3.63 0.001	0 -0.45 0.656	15.5 -2.66 0.012	12 2.34 0.025	1.5 -1.23 0.228	

Key

r^2 adj
t-ratio
p

r^2 adjusted for the number of explanatory variables
|t| > 2 = significant
p < 0.05 means significant within 95% confidence limits
Shading represents significant correlation

Table 4.4 Overview of regresion analysis results for ϕ and c terms.

Explanatory variables	Regression formula	r^2(adj)	Standard dev^n	F test
Cohesion				
$c/\sigma_{fl} = f(\gamma L_x/\sigma_{fl}, Vt/L_x, S, e, \phi, Ar, \sigma_{max}/\sigma_{fl})$	$c/\sigma_{fl} = 0.33(\sigma_{max}/\sigma_{fl})^{1.37}$	78.3	7.01*	120
$c = f(L_i, L_x, \phi, V, \sigma_{fl}, S, e, \gamma, \sigma_{max})$	$c = 16242(L_i) - 7$	70.1	555	73.5
Friction angle				
$\phi = f(\gamma L_x/\sigma_{fl}, Vt/L_x, c/\sigma_{fl}, S, e, Ar, \sigma_{max}/\sigma_{fl})$	$\phi = 0.77 - 2.52(S) + 1.18(e) + 27.7(Vt/L_x)$	45.5	10.6	10.2
$\phi = f(L_i, L_x, c, V, \sigma_{fl}, S, e, \gamma, \sigma_{max})$	$\phi = 1.22 - 168(L_i) + 1.37(e)$	56.4	9.69	21.0
Sensitivity runs (see correlation table also)				
$c = f(\sigma_{max})$	$c = 277 + 0.0897(\sigma_{max})$	62	62.5	51.62
$c = f(\sigma_{max})$	$c = 0.0004(\sigma_{max})^{1.67}$	59.8	1.98*	47.1
$c/\sigma_{fl} = f(\gamma L_x/\sigma_{fl})$	$c/\sigma_{fl} = 39.25(\gamma L_x/\sigma_{fl})^{1.36}$	68.8	10.4*	73.7
excl. Urroz and Ettema (1987), Bruneau (1994a), McKenna *et al.* (1996)				
$c/\sigma_{fl} = f(\gamma L_x/\sigma_{fl}, Vt/L_x, S, e, \phi, Ar, \sigma_{max}/\sigma_{fl})$	$c/\sigma_{fl} = 0.0323 - 0.048(Vt/L_x) - 0.000062(\sigma_{fl}/\sigma_{max})$	55.4	0.0116	14.64
$c = f(L_i, L_x, \phi, V, \sigma_{fl}, S, e, \gamma, \sigma_{max})$	$c = 162 + 17183(L_i) - 18793(V)$	89.8	344	887.8
$\phi = f(L_i, L_x, c, V, \sigma_{fl}, S, e, \gamma, \sigma_{max})$	$\phi = -16.1 - 0.0120(c) + 1.98(e)$	67.2	9.18	21.48

* Standard deviation of natural logarithms.

Table 4.5 Explanatory variable correlation analysis for τ terms.

Key
r^2 adj
r^2 (adj) > 50%
r^2 (adj) > 30%

τ	σn	Li	Lx	V	σ_{fl}	S	e	
77.1								
47.4	45.3							
46.2	43	95						
2.3	1.9	0.7	0.9					
3.1	3.2	15.2	21.8	28.6				
36	37.9	52.8	62.7	1.7	16.5			
3.7	1.6	1.2	0.7	14.1	10.8	4		
5.4	8.3	14.6	18.4	4.2	17	24	33.1	γ

Table 4.6 Explanatory variable correlation analysis for τ terms.

Key
r^2 adj
r^2 (adj) > 50%
r^2 (adj) > 30%

τ/σn	γLx/σn	V*t/Lx	σfl /σn	S	e	
9.9						
3	3.8					
0	14.3	8.8				
0.3	0.4	7.3	6.6			
0	0.4	11.1	11.3	4		
0	2.2	0	10.8	14.8	1.3	Ar

Table 4.7 Overview of regresion analysis results for τ terms.

Explanatory variables	Regression formula	r^2(adj)	Standard dev^n	F test
Shear stress				
$\tau = f(\sigma_n)$	$\tau = 3.52(\sigma_n)^{0.852}$	75.6	0.7221*	1344
$\tau = f(\sigma_n)$	$\tau = 588 + 0.598(\sigma_n)$	77.1	1541	1461
$\tau = f(\sigma_n, L_i, L_x, V, \sigma_{fl}, S, e, \gamma)$	$\tau = 1.05(\sigma_n)^{0.878}(e)^{0.55}/(\sigma_{fl})^{0.0851}$	80.3	0.6482*	591.5
Non-dimensional terms				
$\tau/\sigma_n = f(\gamma L_x/\sigma_n, Vt/L_x, S, e, Ar, \sigma_n/\sigma_{fl})$	$\tau/\sigma_n = 0.651(\gamma L_x/\sigma_n)^{0.201}(Vt/L_x)^{0.104}(S)^{0.054}(e)^{0.464}$	25.2	0.6531	37.37
Sensitivity Runs (incl. or excl. from base data set)				
incl. Cheng and Tatinclaux (1977), Lehmus and Karna (1995)				
$\tau = f(\sigma_n)$	$\tau = 1099 + 0.574(\sigma_n)$	50.9	2295	628.1
$\tau = f(\sigma_n)$	$\tau = 47.9(\sigma_n)^{0.492}$	31.1	1.192*	274.4
$\tau = f(\sigma_n, L_i, L_x, V, \sigma_{fl}, S, e, \gamma)$	$\tau = -748 + 0.566(\sigma_n) + 57.3(e)$	52.1	2267	329.9
excl. Urroz and Ettema (1987), Bruneau (1994a), McKenna *et al.* (1996)				
$\tau = f(\sigma_n)$	$\tau = 1106 + 0.565(\sigma_n)$	73.7	2297	487.5
$\tau = f(\sigma_n)$	$\tau = 18.54(\sigma_n)^{0.638}$	73.3	0.5307*	478.2
$\tau = f(\sigma_n, L_i, L_x, V, \sigma_{fl}, S, e, \gamma)$	$\tau = 0.259(\sigma_n)^{0.612}(e)^{1.29}$	80.0	0.4594*	348.57

* Standard deviation of natural logarithms

Steps
1) Determine rank m of dimension matrix with n parameters (x1-xn)
2) Choose m repeating variables from set of xi, creates matrix A and remainder B (partitions matrix)
3) Invert m x m dimensional matrix A to get C
4) Multiply C and B to get output matrix D
5) extract the n - m Pi parameter (ratios) from D

RELATED PARAMETERS AND THEIR FUNDAMENTAL UNITS

		Length L	Time T	Mass M	Temp θ
Block length	Lx	1	0	0	0
Block thickness	Li	1	0	0	0
Speed	V	1	-1	0	0
Normal stress	σ_n	-1	-2	1	0
Flexural strength	σ_{fl}	-1	-2	1	0
Cohesion	c	-1	-2	1	0
Friction angle	ϕ	0	0	0	0
Specific weight	γ	-2	-2	1	0
Porosity	e	0	0	0	0
Salinity	S	0	0	0	0
Duration	t	0	1	0	0
Aspect ratio	Ar	0	0	0	0
Shear stress	τ	-1	-2	1	0

= Lx / Li

DIMENSIONAL MATRIX

		L	T	M
Bl. length	Lx	1	0	0
Speed	V	1	-1	0
Flex	σ_{fl}	-1	-2	1
Weight	γ	-2	-2	1
Cohesion	c	-1	-2	1
Normal	σ_n	-1	-2	1
Duration	t	0	1	0
Fric.angle	ϕ	0	0	0
Salinity	S	0	0	0
Porosity	e	0	0	0
Aspect ratio	Ar	0	0	0

TRANSPOSE

1) Rank=3

	Lx	V	σ_{fl}	γ	c	σ_n	t	ϕ	S	e	Ar
L	1	1	-1	-2	-1	-1	0	0	0	0	0
T	0	-1	-2	-2	-2	-2	1	0	0	0	0
M	0	0	1	1	1	1	0	0	0	0	0

REPEATING VARIABL | PARTITION | NON-REPEATING

2)

1	1	-1
0	-1	-2
0	0	1

-2	-1	-1	0	0	0	0	0
-2	-2	-2	1	0	0	0	0
1	1	1	0	0	0	0	0

INVERT REPEATING VARIABLE MATRIX

3)

1	1	3
0	-1	-2
0	0	1

-2	-1	-1	0	0	0	0	0
-2	-2	-2	1	0	0	0	0
1	1	1	0	0	0	0	0

MULTIPLY MATRICES

4)

	γ	c	σ_n	t	ϕ	S	e	Ar
Lx	-1	0	0	1	0	0	0	0
V	0	0	0	-1	0	0	0	0
σ_{fl}	1	1	1	0	0	0	0	0

5)

$\gamma Lx/\sigma_{fl}$ | c/σ_{fl} | σ_n/σ_{fl} | $V t/Lx$ | ϕ | S | e | Ar

Figure 4.5 *Matrix method* dimensional analysis for ϕ and c terms.

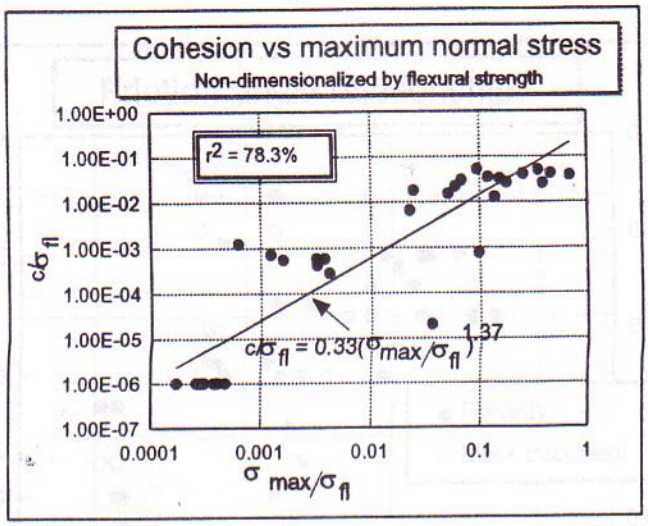

Figure 4.6 Normalized cohesion best-fit regression result.

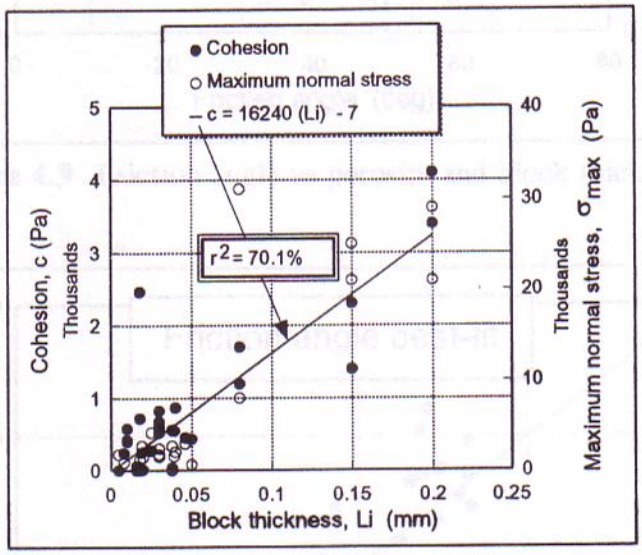

Figure 4.7 Cohesion vs block thickness regression results.

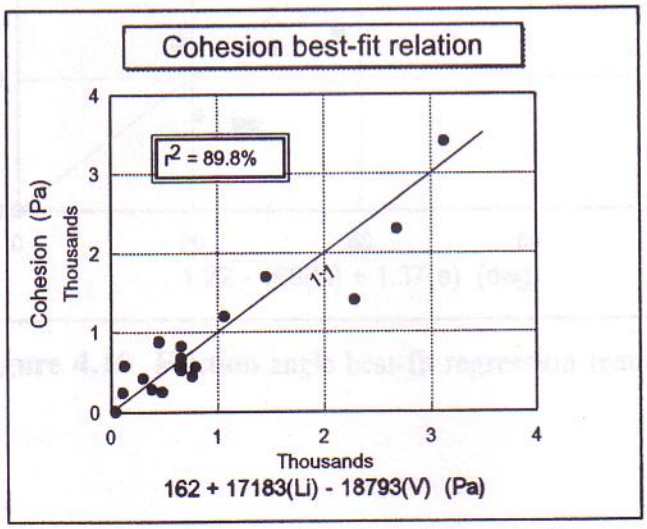

Figure 4.8 Cohesion sensitivity study regression results.

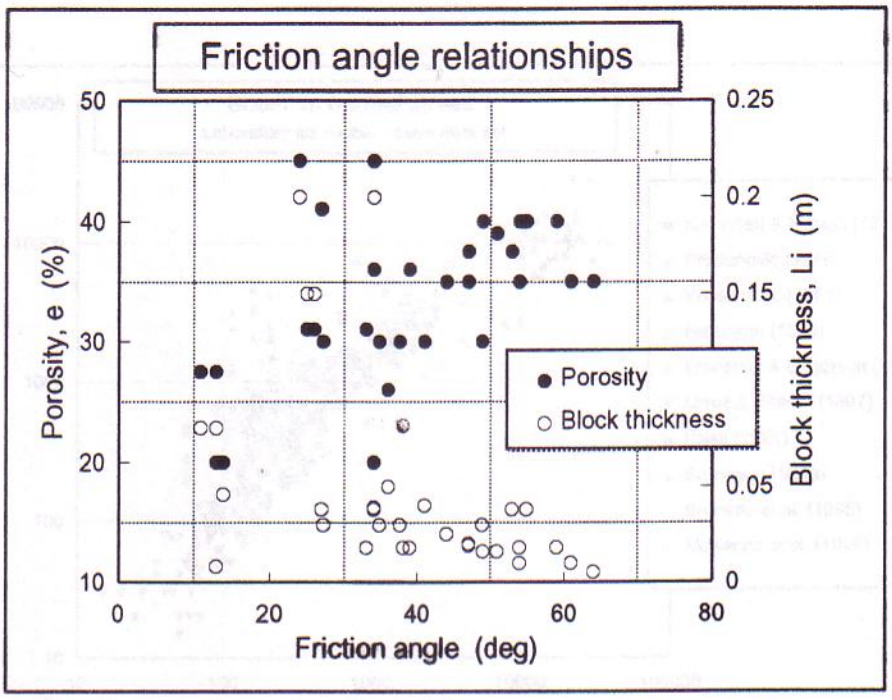

Figure 4.9 Friction angle vs porosity and block thickness.

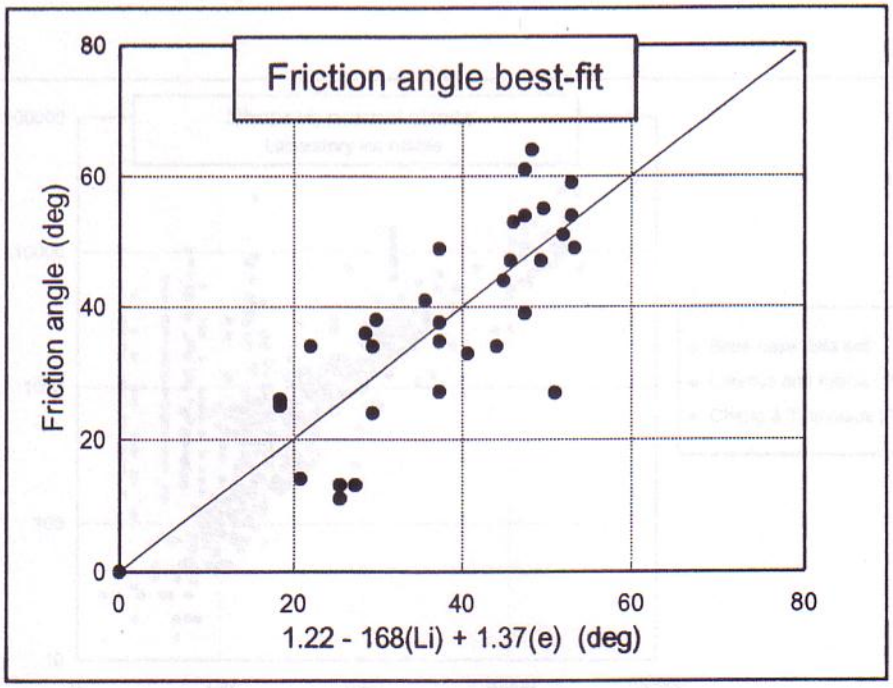

Figure 4.10 Friction angle best-fit regression result.

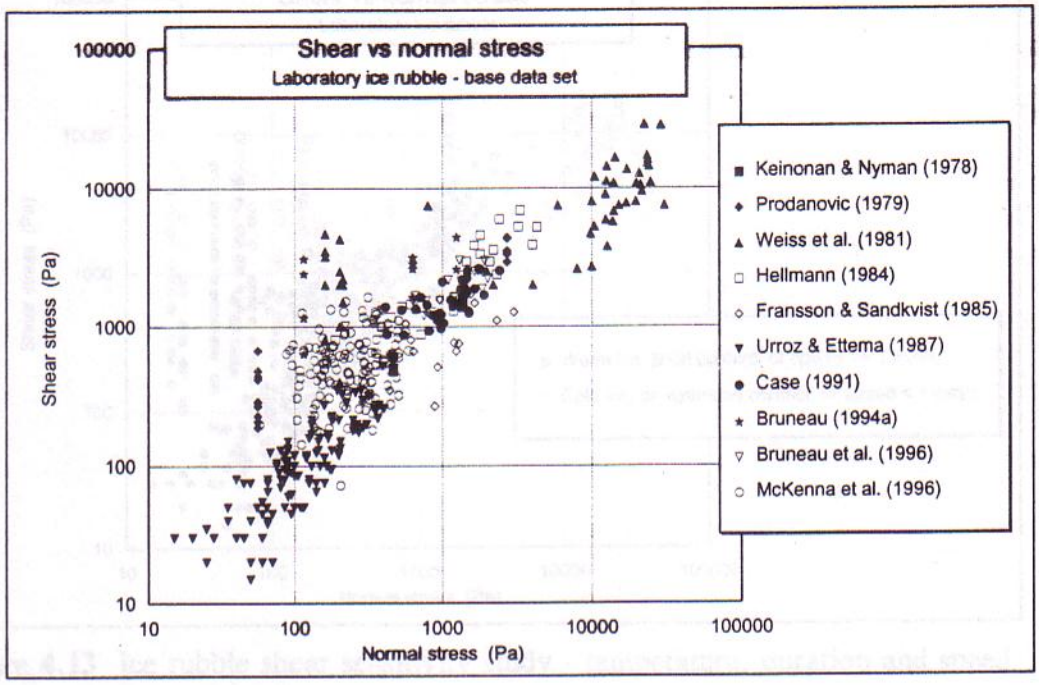

Figure 4.11 Laboratory ice rubble shear vs normal stress data - by author.

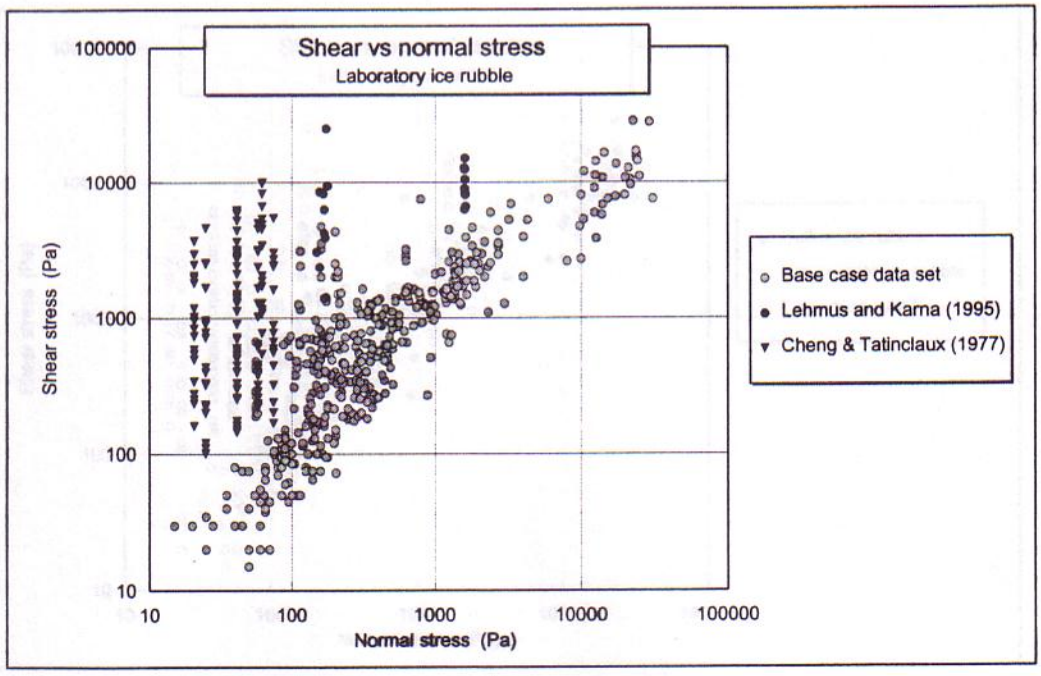

Figure 4.12 Laboratory ice rubble shear vs normal stress data with extreme data.

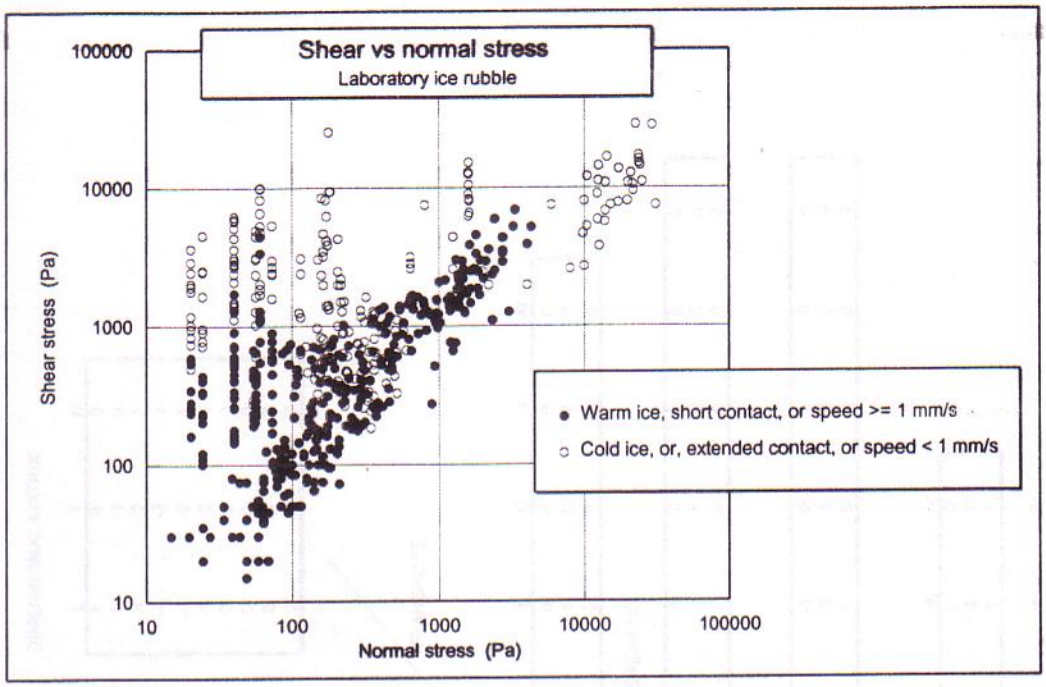

Figure 4.13 Ice rubble shear sensitivity study - temperature, duration and speed.

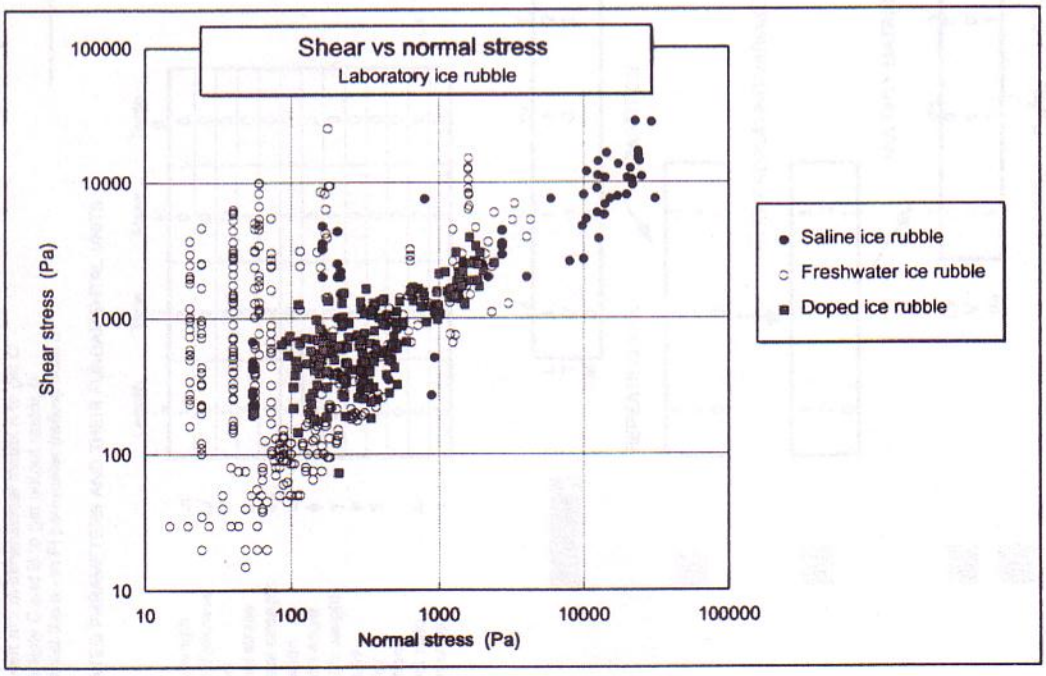

Figure 4.14 Ice rubble shear sensitivity study - ice type.

Steps
1) Determine rank m of dimension matrix with n parameters (x1-xn)
2) Choose m repeating variables from set of xi, creates matrix A and remainder B (partitions matrix)
3) Invert m x m dimensional matrix A to get C
4) Multiply C and B to get output matrix D
5) Extract the n - m Pi parameter (ratios) from D

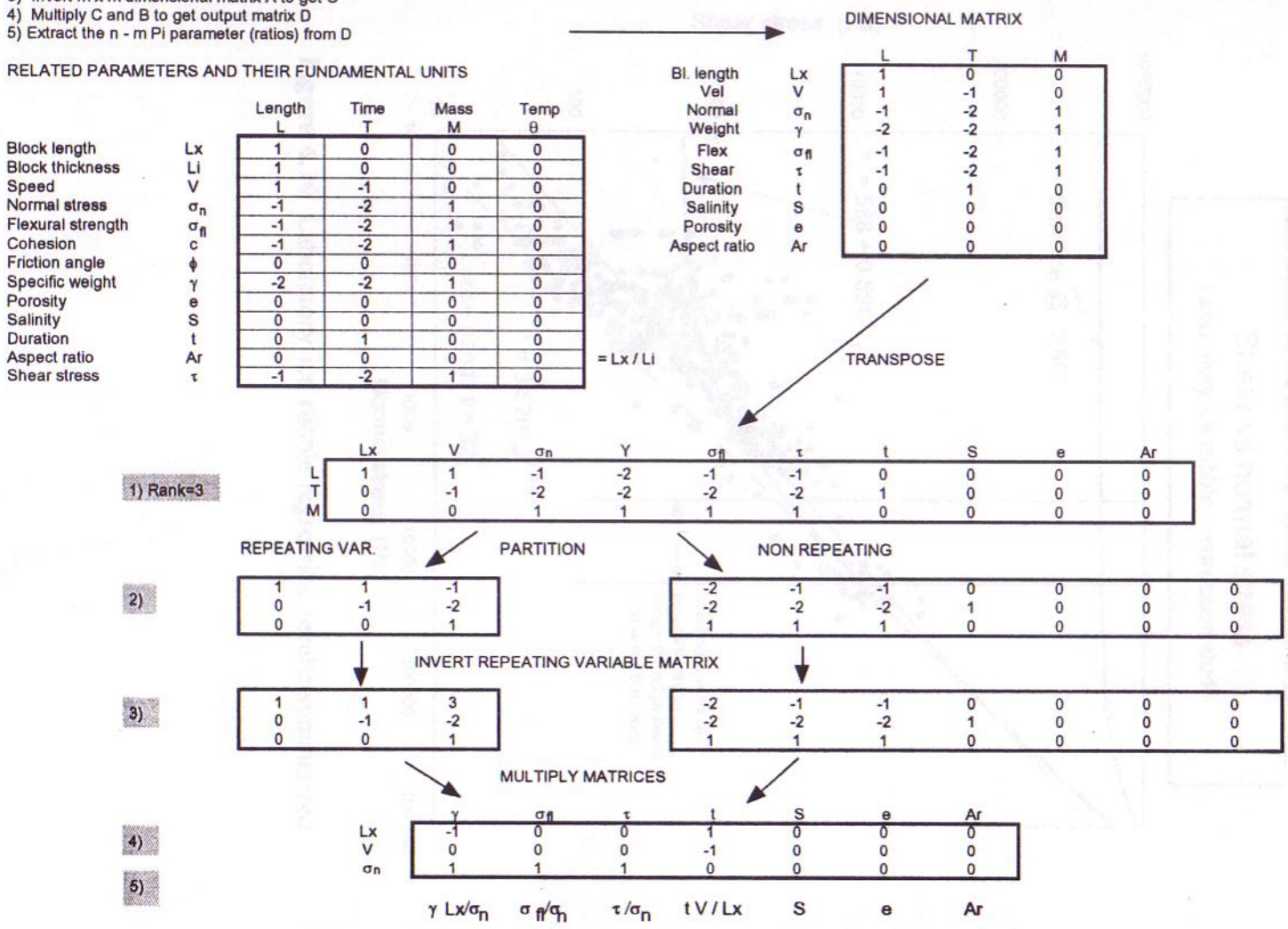

Figure 4.15 *Matrix method* dimensional analysis for τ terms.

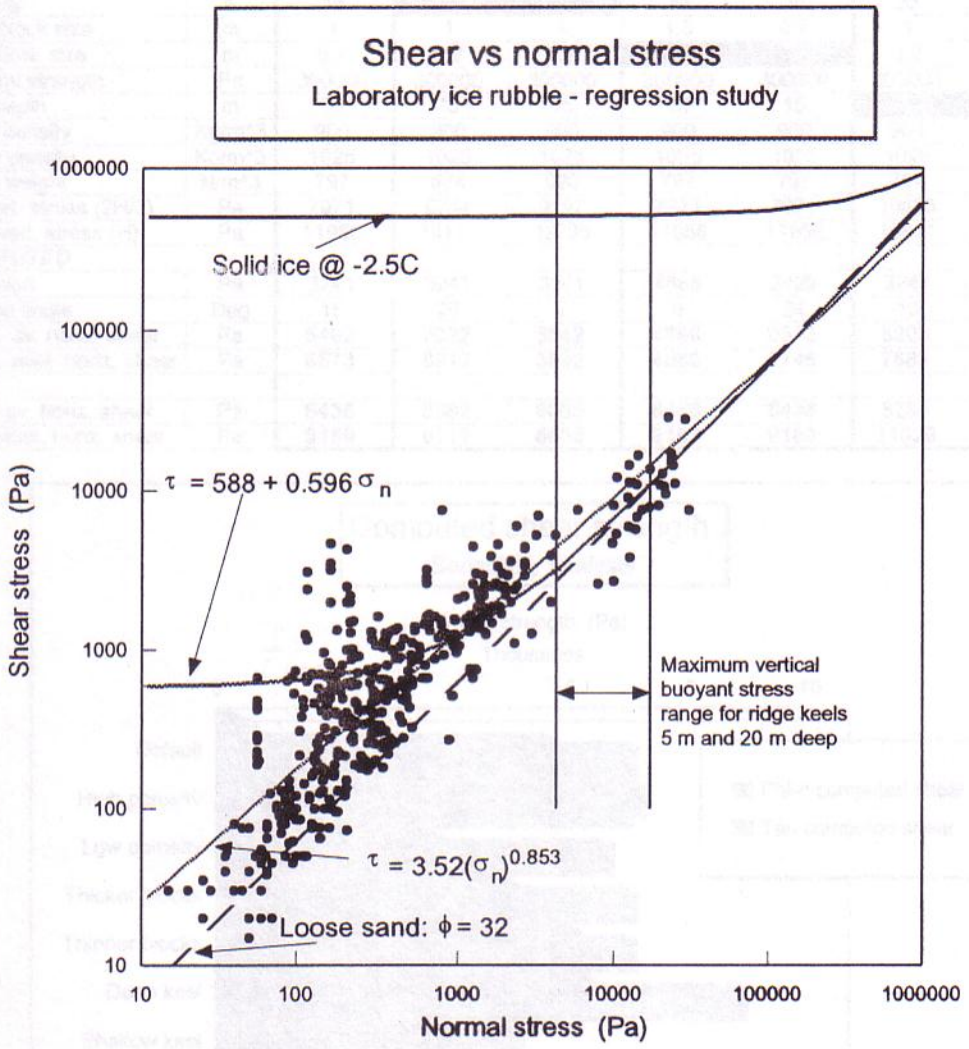

Figure 4.16 Laboratory ice rubble regression results summarized.

Quantity	Units	Default values	Porosity		Block size		Depth	
			high	*low*	*thick*	*thin*	*deep*	*shallow*
Porosity	%	35	45	25	35	35	35	35
Max. block size	m	1	1	1	1.5	0.7	1	1
Min. block size	m	0.2	0.2	0.2	0.3	0.15	0.2	0.2
Flexural strength	Pa	300000	300000	300000	300000	300000	300000	300000
Keel depth	m	15	15	15	15	15	20	10
Block density	Kg/m^3	900	900	900	900	900	900	900
Water density	Kg/m^3	1025	1025	1025	1025	1025	1025	1025
Buoy. weight	N/m^3	797	674	920	797	797	797	797
Av. vert. stress (2H/3)	Pa	7971	6744	9197	7971	7971	10628	5314
Max. vert. stress (H)	Pa	11956	10117	13795	11956	11956	15941	7971
COMPUTED								
Cohesion	Pa	3241	3241	3241	4866	2429	3241	3241
Friction angle	Deg	16	29	2	0	24	16	16
Phi-c - av. horiz. shear	Pa	5462	7022	3542	4866	5973	6203	4722
Phi-c - max. horiz. shear	Pa	6573	8912	3692	4866	7745	7683	5462
Tau - av. horiz. shear	Pa	6436	6382	6065	6436	6436	8286	4509
Tau - max. horiz. shear	Pa	9189	9111	8659	9189	9189	11829	6436

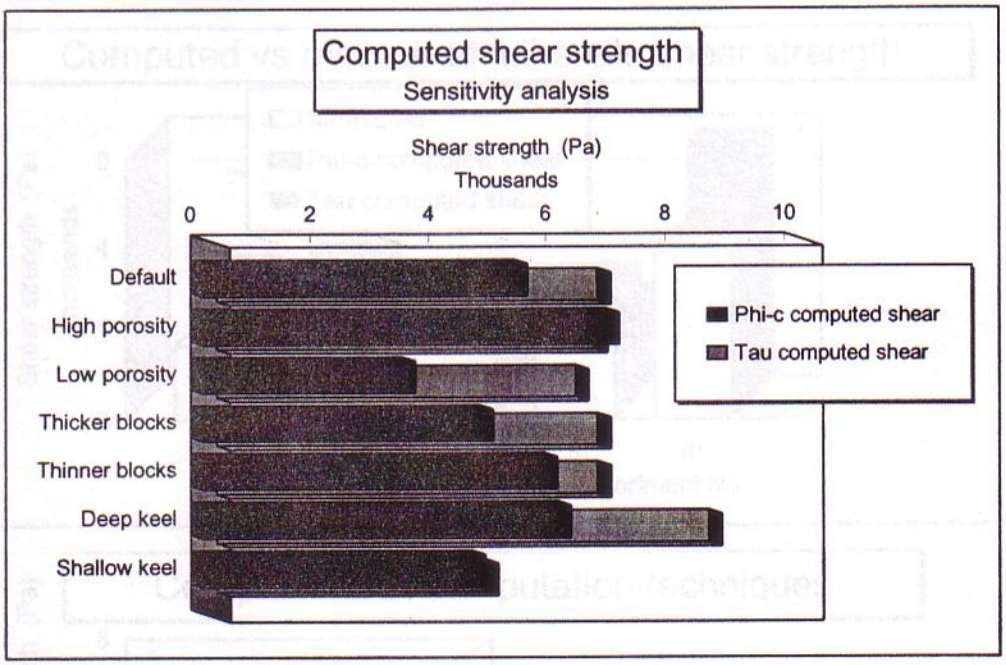

Figure 4.17 Computed ice rubble shear strength - sensitivity study.

Quantity	Units	Lepparanta and Hakala (1992)				
		2	3*	4	5	6*
Porosity	%	23	28	32	33	28
Max. block size	m		0.75	0.6		0.7
Min. block size	m	0.2	0.2	0.11	0.1	0.23
Flexural strength	Pa	300000	300000	300000	300000	300000
Keel depth	m	3.3	3.6	3.9	3.8	11.7
Block density	Kg/m^3	880	880	880	880	880
Water density	Kg/m^3	1025	1025	1025	1025	1025
Buoy. weight	N/m^3	1095	1024	967	953	1024
Av. vert. stress (2H/3)	Pa	2410	2458	2515	2414	7988
Max. vert. stress (H)	Pa	3614	3687	3772	3622	11983
COMPUTED						
Cohesion	Pa	3241	3241	1780	1617	3729
Friction angle	Deg	-1	6	27	30	1
Phi-c - av. horiz. shear	Pa	**3205**	**3499**	**3038**	**2990**	**3860**
Tau - av. horiz. shear	Pa	**1787**	**2027**	**2225**	**2184**	**5704**
MEASURED (from ref.)						
Av. shear strength	Pa	1700	3400	3400	2400	4000

** Failure did not occur therefore stated shear strength is lower bound*

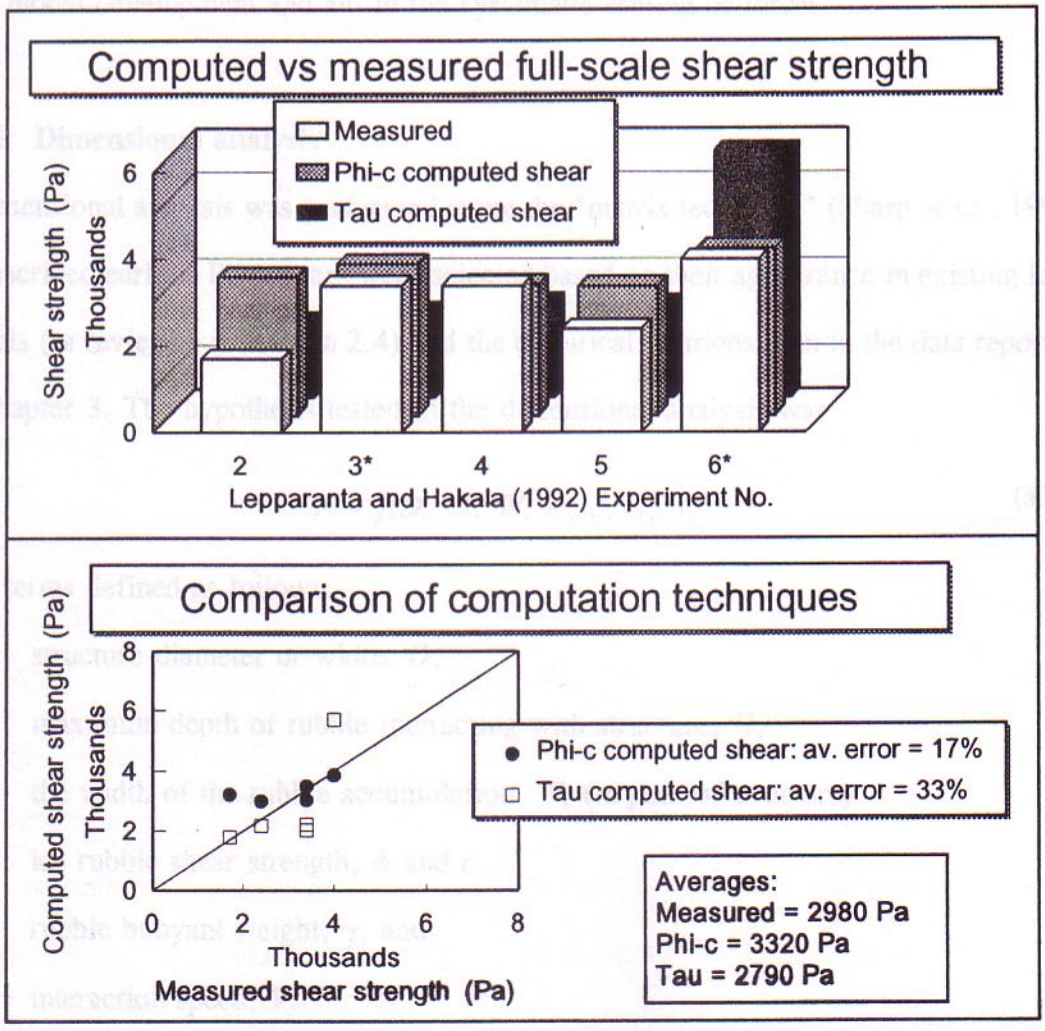

Figure 4.18 Computed ice rubble shear strength - full-scale study.

4.3 Ridge/structure interaction forces

Physical modelling of the interaction between vertical structures and ice rubble has been carried out as part of the work included in this thesis (Bruneau, 1994a, McKenna *et al.*, 1995b, and McKenna, 1996). The purpose has been to establish a basis for load model development. The results of similar work in the literature as reviewed in Section 2.3 have been combined in a regression study in this section. This attempts to determine the correlation between control variables and their relevance to forces measured in laboratory ice rubble/structure interactions. The results provide an empirical basis for theoretical load model development and aid in the systematic scaling of forces.

4.3.1 Dimensional analysis

A dimensional analysis was performed using the "matrix technique" (Sharp *et al.*, 1992) as described earlier. Parameters were selected based on their appearance in existing load models (as reviewed in Section 2.4) and the empirical relations seen in the data reported in Chapter 3. The hypothesis tested in the dimensional analysis was

$$F = f(D,\ H,\ W,\ \phi,\ c,\ \gamma,\ V) \tag{47}$$

with terms defined as follows:

- structure diameter or width, D,
- maximum depth of rubble interacting with structure, H,
- the width of the rubble accumulation, W, (in path of structure)
- ice rubble shear strength, ϕ and c,
- rubble buoyant weight, γ, and
- interaction speed, V.

The shear strength failure criteria are assumed to capture the effect of parameters such

as block size and porosity.

The following dimensionless ratios were formed as shown in Figure 4.19 (with some rearrangements):

$$\frac{F}{\gamma H^2 D} = f\left[\frac{c}{\gamma H}, \phi, \frac{W}{D}, \frac{H}{D}, \frac{W}{H}\right] \tag{48}$$

The last three terms are not mutually independent so that only (any) two of three are of practical importance in a given study.

An alternate approach (Figure 4.20) aimed at involving *speed* in the dimensionless terms yielded

$$\frac{F}{H^2 V^2 \rho} = f\left[\frac{c}{\rho V^2}, \phi, \frac{H}{D}, \frac{W}{D}, \frac{A}{HW}, \frac{gD}{V^2}\right] \tag{49}$$

where g is the gravitational constant, A is ridge cross-sectional area, and ρ is rubble bulk density.

4.3.3 Analysis data set

Table 4.8 is a summary of laboratory ridge/structure interaction data sets. The boundary conditions varied between two-dimensional (wall-to-wall) and three-dimensional (isolated cylinder) indentation, and, from interactions with continuous rubble (modelling a rubble field) to discrete rubble accumulations (modelling a ridge). Also, experiments varied from unconfined (no core present) to confined (with core) horizontal surfaces at the waterline. Cheng and Tatinclaux (1977) did not determine a friction angle for the rubble they used but Mellor (1980) suggested that it was around 46° with very low cohesion

(essentially zero) arbitrarily selected here as 1 Pa. The experiments by Hellmann (1984) involved ploughing a circular vertical plate through rubble under the surface. The boundary condition in this case has been categorized as non-confined although it differs somewhat from those experiments in which structures extend up and out of the water. All experimental results which provide the database for the regression studies reported here are tabulated in Appendix B.

Six scatter plots in Figure 4.21 illustrate the dependency of peak interaction force on the key explanatory variables. A measurement of shear strength is obviously not sufficient for a prediction of interaction forces. There is considerable scatter in the data particularly in the plot of force vs speed, ridge width, rubble buoyant weight and shear strength. It may be possible to argue from these data for a dependency of force on structure diameter, and ridge width but the clearest correlation is a power-law dependency of force on rubble depth. The upward curvature is distinct even without normalization of the other factors. It is important to emphasize that these plots do not isolate the effects of single variables so that no correlations were ruled out prior to the regression study.

4.3.4 Regression study

Multiple regression techniques have been used to synthesize formulas representing the relationship between measured force and the explanatory variables described above. Two groups of dimensionless ratios were investigated for best-fit. The quality of the fitted formulae were determined by the same methods used in the study of ice rubble shear in Section 4.2. Matrix plots and variance inflation factors were used to identify and avoid spurious correlations and multicollinearity problems.

All data sets were grouped for the initial analysis. In the second trial two data sets (Timco and Cornett, 1995, and Bruneau, 1994a "dry tests") were removed. In Timco and Cornett (1995), uncertainty surrounds the non-direct measurement of rubble forces and in Bruneau (1994a) "dry" ice rubble was not submerged. Furthermore neither program had a specified shear strength for ice rubble (in the state tested). In the third trial only those experiments associated with this thesis and reviewed in Chapter 3 were included (Bruneau, 1994a "wet", McKenna *et al.*, 1995a and b, and McKenna, 1996). These tests also correspond to the only data sets which involved discrete ridges for which ridge width and sectional area were reported.

Dummy variables, as suggested by Draper and Smith (1966), were used to quantify the influence of boundary conditions. The three boundary conditions which were identified for this study are, as described above (Subsection 4.3.3): the longitudinal extent or width of the rubble, the lateral extent of the structure and the degree of rubble confinement at the waterline.

Results

A qualitative regression study of the laboratory ridge/structure interaction boundary conditions indicated that only the confinement of the rubble at the waterline significantly affected loads. Neither rubble width nor structure extent were significant factors in measured loads. This result comes as some surprise since the boundary condition which receives the least attention in load models (confinement at the waterline) is the only one of importance in the lab. Results here must be viewed cautiously, however, since the boundary conditions are closely correlated to other laboratory conditions which may also be influential.

Correlation analyses results for all explanatory variables and for each of the three data set groupings are listed in Tables 4.9 to 4.11. Force formulations from the regression analysis are summarized in Table 4.12. Included are the best-fit formulas for both dimensional and non-dimensional explanatory variables. Results which were near best-fit but involved fewer or alternate variables are also given. Both linear and power law best-fit formulas are given with and without intercepts for all three data set groupings.

All data sets

Single variable linear regression results listed in Table 4.9 indicate that force is predominantly influenced by rubble depth and structure diameter. These terms are key elements in "earth pressure" force formulas, $0.5\gamma H^2 D$, and so this was the form (including the 0.5 coefficient) of the normalizing term exploited for subsequent regression tests.

Table 4.12 lists the most significant multi-variable regression results. Although velocity shows up as a significant variable in the first formulation in Table 4.12 it appears later to have an opposite effect (with a different data set). This conflicting result indicates that the significant correlations with velocity are probably arbitrary and coincidental. For most multi-variable regression trials involving dimensional variables those terms associated with hydrostatic "earth pressure" force were again dominant. The term, $0.5\gamma H^2 D$ is the most significant and often the only significant parameter in the regression equations for ridge indentation force. The dependency of indentation force on this term is demonstrated in Figure 4.22 where all data sets are identified by author. The best-fit linear and non-linear formulations invloving only this term are shown in Figure 4.23. According to linear regression results, 93% of the variation in interaction force can be

explained by the following:

$$F = 11.5 \frac{\gamma H^2 D}{2} + 150 \quad \textbf{(50)}$$

The power law relation for the same data set resulted in a 55.7% r^2. The residuals for both are not normally distributed and so the r^2 values are skewed. The plotted results in Figure 4.23 clarify this problem by showing the deviations of both curves from the data points. When the intercept is fixed at zero (for which an r^2 value cannot be interpreted) the apparent fit is better, particularly with the larger scale tests. The formula becomes

$$F = 12 \frac{\gamma H^2 D}{2} \quad \textbf{(51)}$$

All data sets minus Timco and Cornett (1995) and Bruneau (1994a) "dry"

The data set was reduced in size by eliminating the data from Bruneau (1994a) "dry" and Timco and Cornett (1995). Table 4.10 indicates that force is significantly correlated to depth, diameter and internal friction angle. However, ϕ is also correlated to depth and diameter and therefore cannot appear with them as a control term in a multi-variable regression analysis. Regression results indicated an improved linear fit over the previous result. With an $r^2 = 96\%$ the following formula was determined:

$$F = 11.6 \frac{\gamma H^2 D}{2} + 103 \quad \textbf{(52)}$$

The skewness of the residuals for both the transformed power law and linear formulas was diminished somewhat from the previous trial. Plotted results in Figure 4.24 again indicate that the best-fit for the larger scale experiments was a zero-intercept formula with a proportionality coefficient of 12.

Chapter 3 data only (Bruneau, 1994a, McKenna et al., 1995a and b, and McKenna, 1996)

The third regression study was performed on those data sets which involved the indentation of discrete piles of rubble, not continuous rubble fields. Data sets were limited to those reviewed in Chapter 3. Table 4.11 indicates the single variable relationships for this data set and is a guide for avoiding multi-collinearity. Both linear and power-law fits resulted in r^2 values better than 95%. The linear relation established was

$$F = 11.8 \frac{\gamma H^2 D}{2} + 55 \qquad (53)$$

and is shown in Figure 4.25. Again the zero intercept relationship was identical to that for other data sets with a coefficient of 12. Essentially the data sets in this last grouping are directly proportional to hydrostatic earth pressure and form a boundary above which all the other data sets, with quite different boundary conditions, were scattered.

Despite expectations that the width and shear strength of ice rubble accumulations were important factors in determining loads on structures in the lab, regression results indicate otherwise. The non-significant correlations in the multi-variable analysis for these parameters are qualified, however. The close correlation between shear strength and normal stress (a function of rubble buoyant weight and depth) has made the rubble strength terms inseparable from the $0.5\gamma H^2 D$ term. Also, ridge width has a non-zero correlation to depth and so is also inseparable. The robust linear relationship between measured force and $0.5\gamma H^2 D$ with the coefficient of around 12 simply cannot be further reduced or broken down to include other explanatory variables because of these and other

parametric correlations.

4.3.5 Conclusions

In this section a review of experimental results has elucidated the form of fundamental equations describing ridge keel failure forces on vertical structures. Though known, the values of the proportionality coefficients remain somewhat unexplained. The correlation between some of the important experimental conditions has made explaining them difficult. This is a problem for generalizing and scaling results since factors such as ridge width, which may be significant in the laboratory but buried in the proportionality coefficient, may or may not be a significant factor at full-scale.

Motivated by the success of previous "sand keel" tests the next chapter describes a set of control experiments which attempt to reconcile the regression formulas described here with physical modelling results. The rationale is that testing with a material for which shear strength is time-independent and well understood, and with techniques that permit accurate measurements of key experimental conditions, can provide a definitive data set for constructing a working keel force model. A model developed from sand tests would substantially improve existing modelling practices if it could be adapted and calibrated for ice ridge application and still retain the sensitivites to boundary conditions, keel size *etc*. learned with sand.

Table 4.8 Summary of Laboratory ice rubble indentation experiments.

Reference	Boundary conditions			Range of Structural width	Range of Rubble width	Range of Rubble depth	Range of Rubble area	Range of Speed	Range of Peak load	Range of Friction angle	Range of Cohesion
	Rubble extent**	Structure width	Waterline confine.	m	m	m	m^2	m/s	N	deg	Pa
Cheng and Tatinclaux (1977)	C	2-D	N	0.91	Contin*	0.076 -0.22	- na -	0.00015 - 0.0028	19 - 386	46	1
Keinonen & Nyman (1978)	C	2-D	N	0.3	Contin	0.174	- na -	0.025	24	47	10
Prodanovic (1979)	C	3-D	N	0.152 - 0.304	Contin	0.09 - 0.28	- na -	0.001 - 0.009	8 - 285	50	500
Hellmann (1984)	C	3-D	N	0.1	Contin	0.2 - 0.8	- na -	0.001 - 0.25	60 - 600	54 - 61	580 - 420
Timco and Cornett (1995)	D	3-D	Y	0.333	0.8 - 1	0.003 - 0.45	0.002-0.4	0.09 - 0.27	70 - 1900		
Bruneau (1994a) - wet	D	3-D	N	0.114	0.3 - contin.	0.1 - 0.25	.06 - 0.112	0.006	7.5 - 50	50	1500
Bruneau (1994a) - dry	D	3-D	Y	0.114	0.45 - conti	0.1 - 0.2	0.02 - 0.09	0.006	52 - 250		
McKenna et al. (1995a)	D	3-D	N	0.32	2 - 3	0.58 - 0.67	0.59 - 1	0.02 - 0.19	331 - 852	36	500
McKenna et al. (1995a)	D	3-D	Y	0.8	4.5 - 6	0.58 - 1.02	3.4 - 4.2	0.03 - 0.14	870 - 3950	36	500
McKenna (1996)	D	3-D	Y	0.8 - 1.8	1.75 - 6	0.01 - 1	0.014 - 3.1	0.049 - 0.079	610 - 6580	36	873

* Contin. means that rubble was continuous in the direction of structure displacement.
** Rubble extent is either continuous (C) or discrete (D) in the direction of travel

Table 4.9 Explanatory variable correlation analysis - all data sets.

Force (F)	Speed (V)	Depth (H)	Diam (D)	Weight (γ)
20.8				
67.1	30.7			
40.4	3.6	16.8		
0.5	1.7	1.7	4.2	

Key
r^2 adj
r^2 adj > 50%
r^2 adj > 30%

Table 4.10 Correlation analysis for all data minus Timco and Cornett (1995), and Bruneau (1994a) "dry".

Force (F)	Speed (V)	Depth (H)	Diam (D)	Weight (γ)	Friction (ϕ)	Cohesion (c)
22.6						
68.3	43.6					
40.6	5.7	14.9				
1.8	0.4	0	0			
30.4	28.4	36.2	40.4	3.8		
3.4	0	0	25.3	0	8.8	

Key
r^2 adj
r^2 adj > 50%
r^2 adj > 30%

Table 4.11 Correlation analysis of Chapter 3 data sets only.

Force (F)	Speed (V)	Depth (H)	Diam (D)	Weight (γ)	Friction (ϕ)	Cohesion (c)	Area (A)	Width (W)
1.9								
58.2	24.4							
52.3	0	28.1						
3.1	5.7	0	5.7					
8.5	16.4	43.7	13.1	10.2				
33.8	12.5	56.3	43	1.8	45			
36.2	28.3	53.8	23.8	2.4	14.7	43.6		
33	19.7	52	30.7	0	34.9	55.3	81.2	

Key
r^2 adj
r^2 adj > 50%
r^2 adj > 30%

Table 4.12 Summary of regression results for structure interaction tests.

Structure tests: explanatory variables	Regression formula	r^2 (adjusted)	Std. dev^n	F test
All data sets				
$F = f(D, H, V, \gamma, g)$	$F = 4820H^{0.695}D^{0.7}V^{0.283}$	68.0	0.9436*	85.86
$F = f(\gamma H^2D, H/D, gD/V^2)$	$F = 11.5(0.5\gamma H^2D) + 49.1(H/D) + 82.6$ $F = 337(0.5\gamma H^2D)^{0.521}(H/D)^{-.375}(gD/V)^{-.147}$ $F = 11.5(0.5\gamma H^2D) + 150$ $F = 82.3(0.5\gamma H^2D)^{0.504}$	93.1 66.9 92.8 55.7	304 0.9586* 310 1.11*	810 82.0 151.9
$F = f(\gamma H^2D)$ without intercept	$F = (0.5\gamma H^2D)^{1.34}$ $F = 12.1 * 0.5\gamma H^2D$		3.796* 337	137.4 1800
Minus: Timco and Cornett (1995), Bruneau (1994a) "dry"				
$F = f(D, H, V, \gamma, g, \phi, c)$	$F = 3413H + 1710D + 3.43\gamma + 62.3\phi - 6528$ $F = 780H^{1.75}D^{.903}c^{-.151}V^{-.245}$	88.9 86.8	412 0.6357*	203 166.4
$F = f(\gamma H^2D, H/D, gD/V^2, \phi, c/\gamma H)$	$F = 11.7(0.5\gamma H^2D) + 60.2(H/D) + 16.2$ $F = 11.6(0.5\gamma H^2D) + 103$ $F = 47.0(0.5\gamma H^2D)^{.731}$	96.8 96.4 84.7	220 236 0.6836*	1539 2671 559
$F = f(\gamma H^2D)$ without intercept	$F = (0.5\gamma H^2D)^{1.6}$ $F = 12.0 * 0.5\gamma H^2D$		3.0* 252	244 3185
Chapter 3 data sets only: Bruneau(1994a) "wet", McKenna et al. (1995b), McKenna (1996)	* Standard deviation of natural logarithms			
$F = f(D, H, V, \gamma, g, \phi, c, W, A)$	$F = 38.1\gamma^{0.708}H^{1.87}D^{0.969}$	97.3	0.3103*	412
$F = f(\gamma H^2D, H/D, gD/V^2, \phi, c/\gamma H, W/D, A/WH)$	$F = 15.6(0.5\gamma H^2D)^{0.944}$ $F = 11.8(0.5\gamma H^2D) + 54.6$	97.4 95.3	0.3035* 348	1291 695.34
$F = f(\gamma H^2D)$ without intercept	$F = (0.5\gamma H^2D)^{1.5}$ $F = 12.0 * 0.5\gamma H^2D$		1.232* 344	1064 1697

Steps

1) Determine rank m of dimension matrix with n parameters (x1-xn)
2) Choose m repeating variables from set of xi, creates matrix A and remainder B (partitions matrix)
3) Invert m x m dimensional matrix A to get C
4) Multiply C and B to get output matrix D
5) Extract the n - m Pi parameter (ratios) from D

RELATED PARAMETERS AND THEIR FUNDAMENTAL UNITS

		Length L	Time T	Mass M
Pier Diameter	D	1	0	0
Keel Width	W	1	0	0
Keel Depth	H	1	0	0
Keel Area	A	2	0	0
Keel Aspect ratio	Ar	0	0	0
Speed	V	1	-1	0
Rubble Buoy	γ	-2	-2	1
Rubble Density	ρ	-3	0	1
Gravity constant	g	1	-2	0
Shear strength	τ	-1	-2	1
Cohesion	c	-1	-2	1
Friction angle	ϕ	0	0	0
Pier Force	F	1	-2	1

DIMENSIONAL MATRIX

		L	T	M
Diam	D	1	0	0
Speed	V	1	-1	0
Buoy	γ	-2	-2	1
Cohesion	c	-1	-2	1
Force	F	1	-2	1
Width	W	1	0	0
Depth	H	1	0	0
Friction An.	ϕ	0	0	0

TRANSPOSE

	D	V	γ	c	F	W	H	ϕ
L	1	1	-2	-1	1	1	1	0
T	0	-1	-2	-2	-2	0	0	0
M	0	0	1	1	1	0	0	0

1) Rank=3

REPEATING VAR. PARTITION NON REPEATING

2)

1	1	-2
0	-1	-2
0	0	1

-1	1	1	1	0
-2	-2	0	0	0
1	1	0	0	0

INVERT REPEATING VARIABLE MATRIX

3)

1	1	4
0	-1	-2
0	0	1

-1	1	1	1	0
-2	-2	0	0	0
1	1	0	0	0

MULTIPLY MATRICES

4)

	c	F	W	H	ϕ
D	1	3	1	1	0
V	0	0	0	0	0
γ	1	1	0	0	0

5) π groups $c/\gamma D$ $F/\gamma D^3$ W/D H/D ϕ

Figure 4.19 *Matrix method* dimensional analysis no. 1 for interaction force terms.

Steps
1) Determine rank m of dimension matrix with n parameters (x1-xn)
2) Choose m repeating variables from set of xi, creates matrix A and remainder B (partitions matrix)
3) Invert m x m dimensional matrix A to get C
4) Multiply C and B to get output matrix D
5) Extract the n - m PI parameter (ratios) from D

RELATED PARAMETERS AND THEIR FUNDAMENTAL UNITS

		Length L	Time T	Mass M
Pier Diameter	D	1	0	0
Keel Width	W	1	0	0
Keel Depth	H	1	0	0
Keel Area	A	2	0	0
Keel Aspect ratio	Ar	0	0	0
Speed	V	1	-1	0
Rubble Buoy	γ	-2	-2	1
Rubble Density	ρ	-3	0	1
Gravity constant	g	1	-2	0
Shear strength	τ	-1	-2	1
Cohesion	c	-1	-2	1
Friction angle	ϕ	0	0	0
Pier Force	F	1	-2	1

DIMENSIONAL MATRIX

		L	T	M
Diam	D	1	0	0
Speed	V	1	-1	0
Density	ρ	-3	0	1
Cohesion	c	-1	-2	1
Force	F	1	-2	1
Width	W	1	0	0
Depth	H	1	0	0
Area	A	2	0	0
Gravity	g	1	-2	0
Friction an.	ϕ	0	0	0

TRANSPOSE

	D	V	ρ	c	F	W	H	A	g	ϕ
L	1	1	-3	-1	1	1	1	2	1	0
T	0	-1	0	-2	-2	0	0	0	-2	0
M	0	0	1	1	1	0	0	0	0	0

1) Rank=3

REPEATING VAR. PARTITION NON REPEATING

2)

1	1	-3	-1	1	1	1	2	1	0
0	-1	0	-2	-2	0	0	0	-2	0
0	0	1	1	1	0	0	0	0	0

INVERT REPEATING VARIABLE MATRIX

3)

1	1	3	-1	1	1	1	2	1	0
0	-1	0	-2	-2	0	0	0	-2	0
0	0	1	1	1	0	0	0	0	0

MULTIPLY MATRICES

4)

	c	F	W	H	A	g	ϕ
D	0	2	1	1	2	-1	0
V	2	2	0	0	0	2	0
ρ	1	1	0	0	0	0	0

5)

π groups $c/\rho V^2$ $F/(\rho(DV)^2$ W/D H/D A/D^2 gD/V^2 ϕ

Figure 4.20 *Matrix method* dimensional analysis no. 2 for interaction force terms.

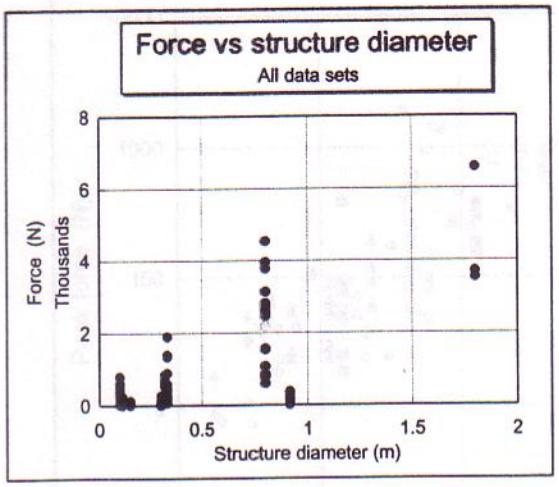

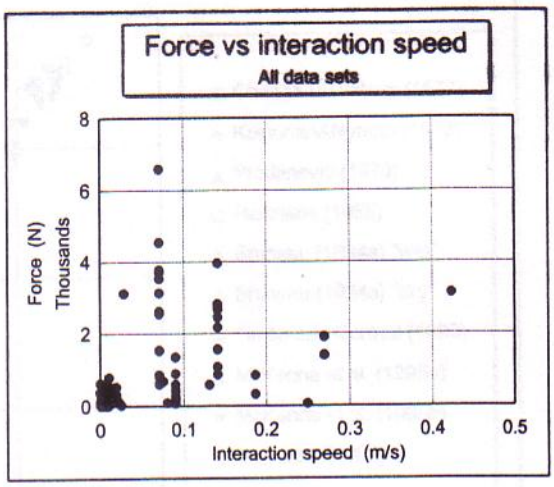

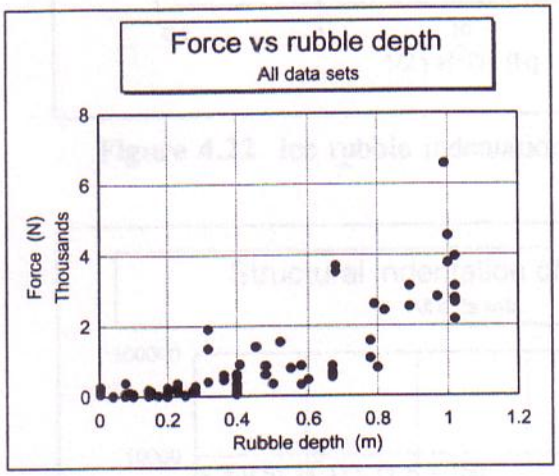

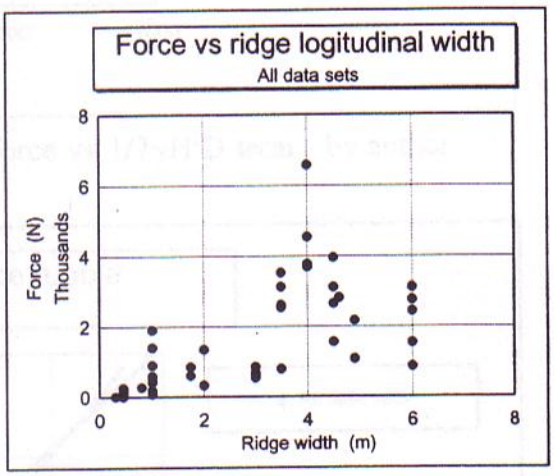

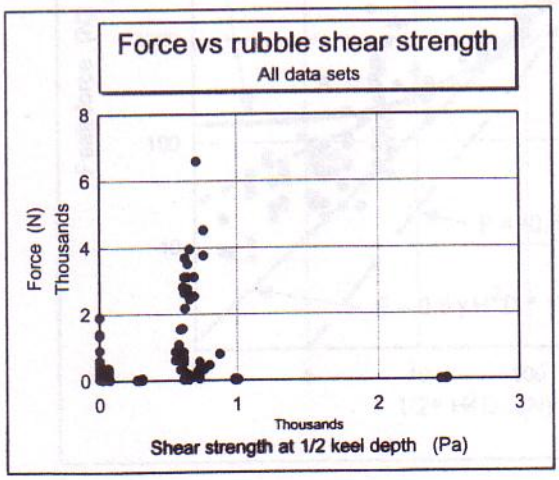

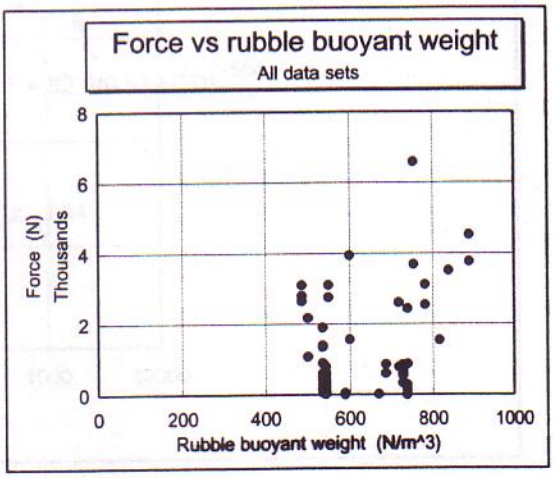

Figure 4.21 Scatter plots of force versus key variables.

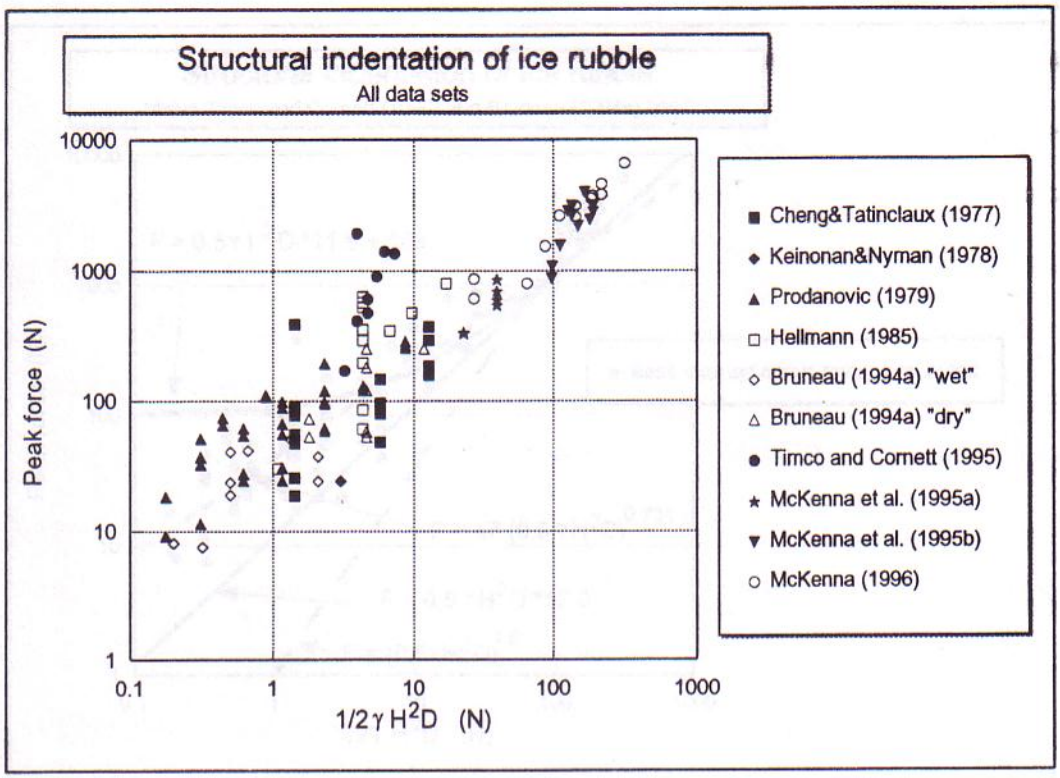

Figure 4.22 Ice rubble indentation force vs $1/2\gamma H^2D$ term - by author.

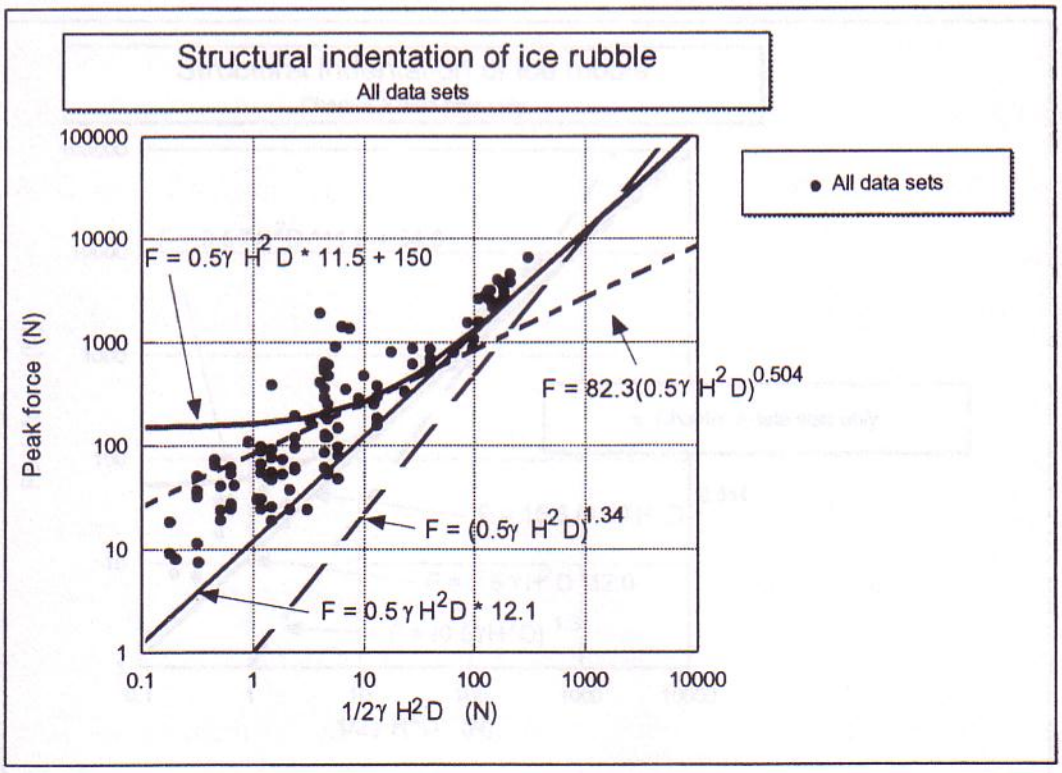

Figure 4.23 Ice rubble indentation force vs $1/2\gamma H^2D$ term - regression results.

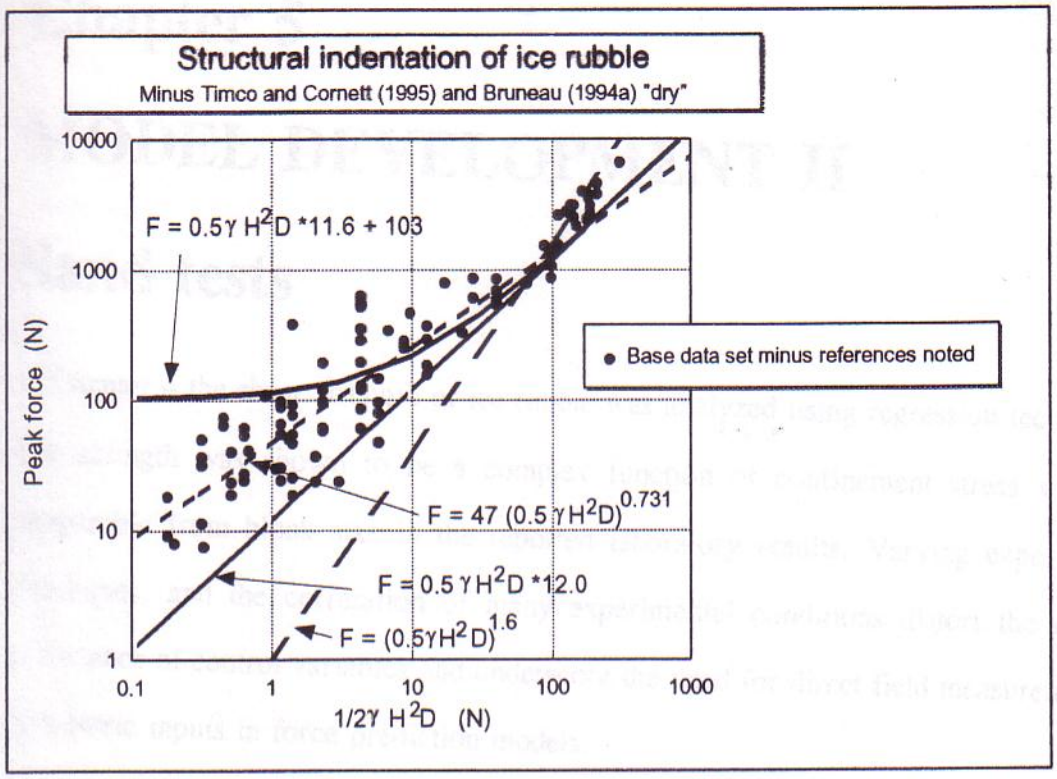

Figure 4.24 Ice rubble indentation force vs $1/2\gamma H^2D$ term - sensitivity study.

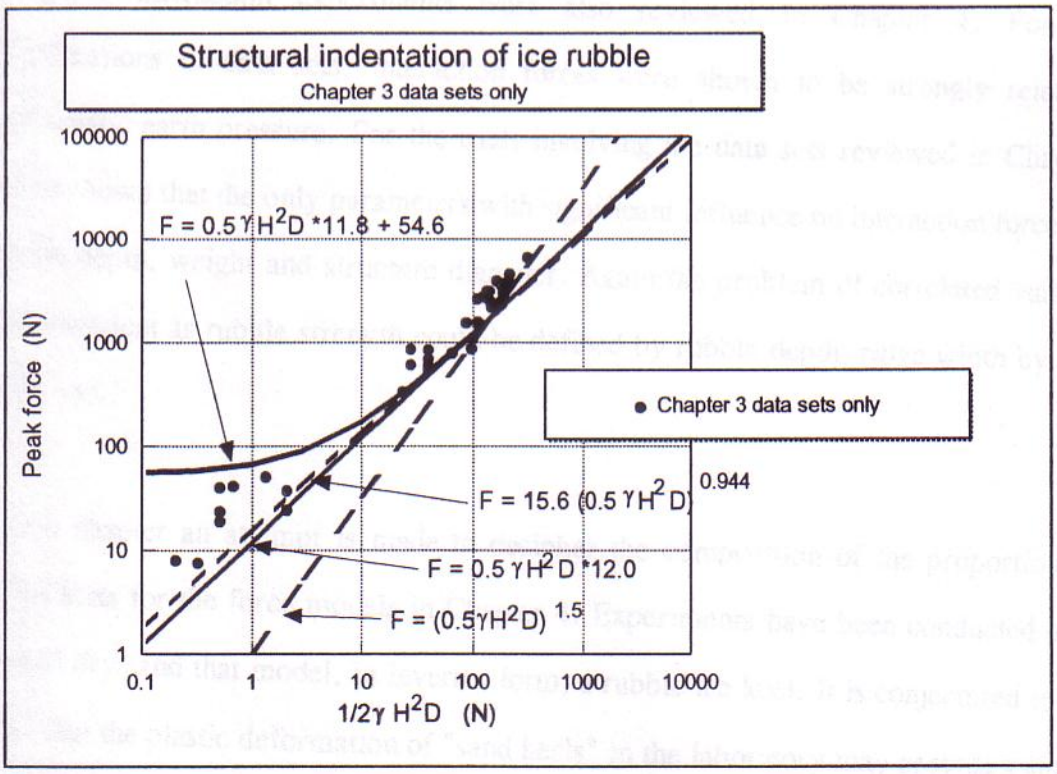

Figure 4.25 Ice rubble indentation force vs $1/2\gamma H^2D$ term - sensitivity study.